QATAR UNIVERSITY

COLLEGE OF ENGINEERING

A NUMERICAL AND EXPERIMENTAL INVESTIGATION OF A SPECIAL TYPE OF FLOATING-SLAB TRACKS

BY

SATEH ABDULNASER ALABBASI

A Thesis Submitted to

the Faculty of the College of Engineering

in Partial Fulfillment of the Requirements for the Degree of

Master of Science in Civil Engineering

June 2019

COMMITTEE PAGE

The members of the Committee approve the Thesis of
Sateh Abdulnaser Alabbasi defended on 16/04/2019.

Dr. Mohammed F Hussein
Thesis/Dissertation Supervisor

Dr. Pedro Galvín
Committee Member

Dr. Asan Abdul Muthalif
Committee Member

Dr. Murat Gunduz
Committee Member

Approved:

Abdel Magid Hamouda , Dean, College of Engineering

ABSTRACT

ALABBASI, SATEH, A., Masters: June : 2019,

Masters of Science in Civil Engineering

Title: A Numerical and Experimental Investigation of A Special Type of Floating-Slab Tracks

Supervisor of Thesis: Dr. Mohammed, F, Hussein.

This thesis presents a research study on the dynamic behavior of a special type of FST used in recently built subway system in Doha, Qatar. The special FST has a continuous concrete slab with periodic grooves for which the track can be modeled as periodic structure with a slab unit having two elements with different cross sections. Extensive numerical and experimental investigations were conducted on a multi-unit full-scale mockup track. The numerical investigations were carried out using both a fast running model based on the Dynamic Stiffness Method and a detailed Finite Element model. In the experimental campaign, experimental vibration test was performed to identify the actual vibration response of the mockup track. Results from the experimental investigations were then used for verifying the numerical models and carrying out a model updating exercise for the fast running model. The model updating process was carried out according to an automated hybrid optimization approach. Finally, the updated model was extended to an infinite model and used in a parametric study to investigate the influence of varying groove's thickness on the dynamic behavior of the special track with infinite length for both bending and torsion scenarios. The parametric study suggested that reducing the thickness below 50% of the full thickness of the slab significantly affects the dynamic behavior of the special FST.

DEDICATION

To my grandparents, parents, family, wife and son.

ACKNOWLEDGMENTS

At the beginning, I would like to sincerely thank Allah for giving me the limitless strength, blessings, endurance and knowledge to finalize this study.

I am grateful to my research supervisor Dr. Mohammed Hussein for his continuous support during my undergraduate and graduate studies at Qatar University. I would like to thank him from the bottom of my heart for his patience, inspiration and enthusiasm during my studies. I thank him for his supportive contributions to enhance my level of knowledge during my studies. I would like to show my sincere and deep feeling thankfulness to him for being as a great brother before being my supervisor.

I am grateful to Dr. Osama Abdeljaber the research assistant in the Civil and Architectural department at Qatar university for developing the finite element model and carrying out the hybrid optimization process in this thesis.

I am grateful to Qatar Rail for giving me the permission to access to the mockup track site and for providing me the required drawings and information.

Finally, I would like to show my grateful thanks to my parents, family and my wife for their endless support, motivation and great sacrifice to complete this study.

TABLE OF CONTENTS

LIST OF TABLES

LIST OF FIGURES

CHAPTER 1:RESEARCH BACKGROUND

1.1 Introduction

The main purpose of railway trains is to transport large number of passengers and goods. The rate of degradation of railway tracks should be reduced to minimize the maintenance activities and the associated financial and social impacts. Degradation of tracks are influenced by the track dynamics. Track dynamics also affects the ride quality and the levels of emission of noise and vibrations perceived by passengers. The dynamic interactions between the components of railway tracks influence the structural integrity of the track and the levels of noise and vibrations transmitted to buildings in proximity. Several studies have shown that such vibrations have significant effects on human health and comfort [1-4]. Railway-induced vibrations can also damage sensitive equipment [5, 6] and historical buildings [7].

Investigating the dynamic behavior of railway tracks is important to preserve and maintain the track in a good condition and reduce the results of the track dynamics on the track's structure, trains' passengers and the nearby structures. To improve the understanding of the dynamic behavior of the railway track and its components, the railway tracks are modelled using different numerical methods and techniques. Railway numerical models can capture the dynamic behavior of railway tracks.

There are two main types of railway tracks, ballast tracks and slab tracks. The obvious difference between the two types of tracks is the material used for the track bed. In the ballast tracks the rails are mounted on a discontinuous rail pads supported via horizontal sleepers resting on a graded granular gravel called ballast (Figure 1). For slab tracks the rails are supported via rail resilient elements rested on a concrete slab supported by track foundation (Figure 2).

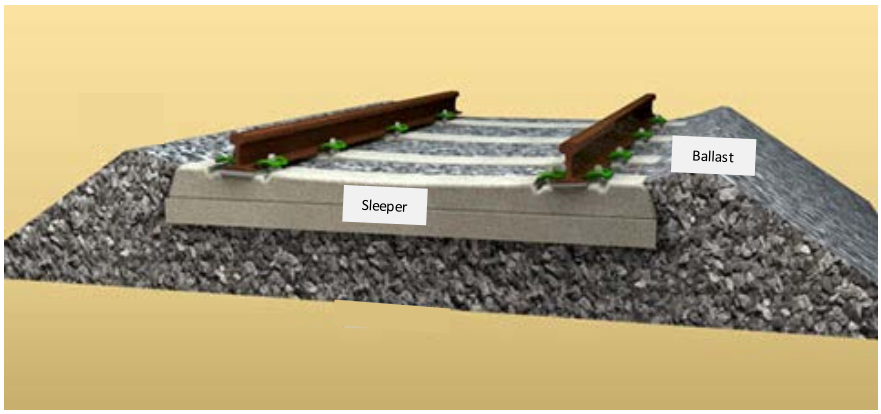

Figure 1: Cross section view of ballast tracks [8].

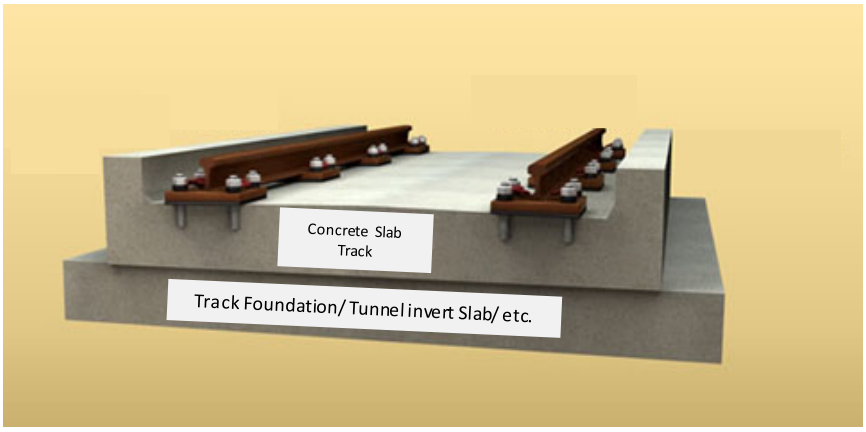

Figure 2: Cross section view of slab tracks [8].

Floating-slab tracks (FSTs) are commonly used for controlling railway-induced vibrations. In FSTs, the concrete slab rest on resilient elements called slab bearings. Slab bearings have an important role of improving levels of vibration isolation [9-12]. The concrete slab can be either continuous or discontinuous. In continuous concrete FSTs, the concrete is poured in site. While for discontinuous FSTs, precast concrete units are used. The continuous slab system in Washington DC is an example of

continuous FST. New York subway (7 m slab units) is an example of discontinuous FST [13].

A special FST design was adopted in the State of Qatar railway network (Doha Metro) that consists of 100 stations and 4 lines with a total distance of 300 km. The track consists of a continuous slab with periodic grooves along the track as show in Figure 1. The repeating concrete slab unit consist of two segments with different cross sections. The purpose of this track design is to allow cables crossings and to facilitate the installation of shuttering required for casting of grout in between the slabs.

Figure 3: Groove in the concrete floating slab.

1.2 Problem Statement

A special FST that has a continous concrete slab with intervallic grooves need to be investigated. This type of FST cannot be accurately modeled using the previous reported continuous and discontinuous numerical models which assume a constant

cross-section along the slab unit. The slab unit in this type of track is consisting of two segments with different cross sections.

1.3 Aim of The Thesis

This thesis aims to investigate the influence of varying the groove thickness- which in turn is going to vary the slab segments' parameters- on the dynamic behavior of full infinite track.

1.4 Thesis Outline

The rest of the thesis is organized as follows. Chapter 2 reviews the related reported work in the literature. Chapter 3 describes the numerical model's formulation for the fast running model and Finite Element (FE) model. Chapter 4 shows the verification of the numerical models by comparing obtained results from the fast running model with the FE model. Also, it shows the validation of the results of the fast running model with the experimental test results conducted on the mockup structure. Furthermore, it includes the updating process of the fast running model. Chapter 5 describes the parametric study conducted to understand how the vibration response of the railway track is affected by varying grooves thickness along the track. Finally, Chapter 6 concludes the work of thesis.

CHAPTER 2:LITERATURE REVIEW

2.1 Introduction

This chapter reviews the literature that is relevant to this thesis. This includes the previous work related to the numerical models of the railway tracks and the conducted experimental vibration measurements on different railway tracks.

2.2 Numerical Models

This section reviews the relevant numerical models reported in the literature. The section is organized in the following sub-sections: beam theories used in the numerical railway track models, numerical models of railway track as single continuous and discontinuous beam, double beam layer railway track models and FSTs numerical models for continuous and discontinuous FSTs.

2.2.1 Beam Theories Used for Track Models

Hetényi [14] showed that Winkler modeled the railway track as an infinite single beam on elastic homogeneous foundation. For the stiffness of the elastic homogeneous foundation used in Winkler model, Kerr [15] provided a design curves to determine the empirical stiffness value based on the deflections measured under known axel loads. Despite the age of this model, many researchers still using it to study many areas related to track dynamics due to its simplicity. Winkler beam has been modelled for different beam theories to study dynamics of railway tracks.

One of the most common theories used of Winkler beam model is Euler Bernoulli beam theory to study dynamic properties of beams [16].Jacob Bernoulli in the 18th century presented this theory which was later used by Leonard Euler to study elasticity of the beams. The theory's main assumption is that, the plane sections continue plane and vertical to the neutral axis after the load application (Figure 4). If the cross section is less than the wavelength of the motion, this theory is applicable. Hence, for investigating railway tracks dynamics at high frequency above 500 Hz which

is approximately the maximum frequency of validity [17], this theory is not applicable as it overestimate the natural frequency of the beam when it is calculated. This is because of the rotational inertia and shear deformation effect and it is significant to be taken into consideration.

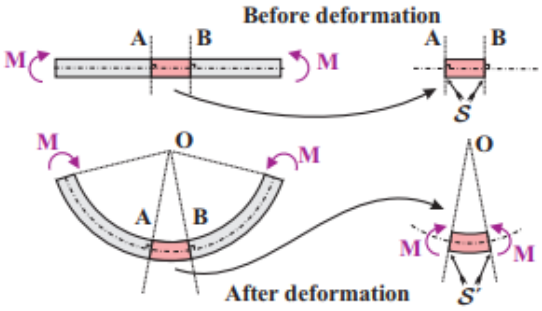

Figure 4: Euler Bernoulli beam theory [18].

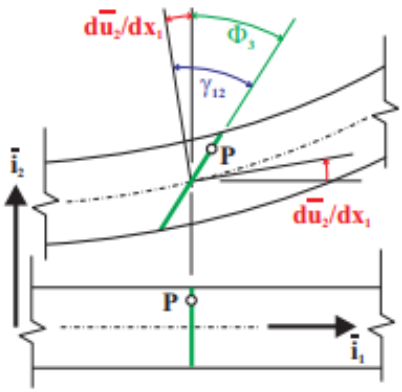

Figure 5: Timoshenko beam theory [18].

Lord Rayleigh [19] included the rotational inertia effect on the previous beam theory. However, his model did not provide correct results of the natural frequencies for higher frequencies of motion, it is still overestimated. Shear deformation should be introduced to improve the calculations of natural frequencies of a beam. Timoshenko [20, 21] presented a beam theory accounting for both rotational inertial (Φ) and shear deformation (γ) of a beam (Figure 5) leading for better calculations of natural frequencies of a beam in a range of high frequency applications. Thus, this theory is valid for high frequency railway track applications which extend up to 5kHz [22] . For investigating dynamic behavior of railway tracks, frequency is dependent factor of this investigations. Based on the frequency range of interest the used beam theory is determined for example for studies interested in ground vibration the up limit of the interested frequency is up to 250 Hz [23], where Euler Bernoulli theory is applicable. In the other side, studying rolling noise occurrences is an example of an application in such the interested frequency range extends to 5 kHz [24], where Timoshenko beam theory is applied.

Chonan [25] used Timoshenko beam theory to model a beam on elastic undamped foundation. In his paper, Chonan introduced small damping to the foundation to shift the poles to the complex domain. A comparison between responses of Euler Bernoulli beam and Timoshenko beam models has done by Bogacz et al. [26].

2.2.2 Railway Tracks Models

Railway track models can be categorized in two main categories based on the beam layer, aiming to represent the two main types of tracks: ballast tracks and slab tracks. As those with single beam models are used generally to investigate ballast tracks. Where, those with double beam models are used to model Slab tracks. However, some researchers used double beam model to model ballast tracks.

Single beam models

Single beam models can be classified to two classifications based on the continuity nature of the beneath supporting layer (Figure 6). The supporting layer can be modelled as continuous or discontinuous supporting layer [17].

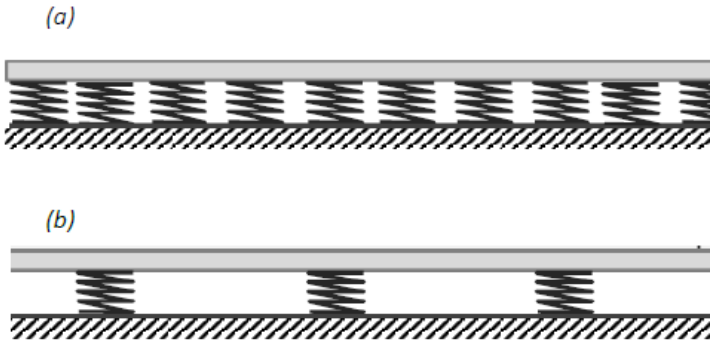

Figure 6: Single beam models with, (a) continuous and (b) discontinuous supporting layer [17].

Single continuous beam models

Mathews [27] modeled Euler Bernoulli beam on infinite elastic foundation without damping and he used Fourier transformation method to solve the beam's differential equation. For the beam response he used Contour Integrals and Residue Theorem to calculate closed form solution. In his paper, the results are found for the case of complex poles i.e. for velocities below critical velocity. In another paper Mathews [28] manipulate the response in the presence of viscous damping including moving load with all velocities and excitation frequencies. The results show that all the poles are complex. In his paper, he found out special characteristics for the case of a

beam on elastic foundation without damping effect. The first one, is for velocities above critical velocity, purely real poles are founded. The other one, is that in a moving frame of reference, the displacements are symmetrical about non-oscillating moving.

The steady-state solution of a damped beam on elastic foundation due to a non-oscillating moving load is investigated by Kenny [29]. The author takes into account velocities overhead critical velocity in his investigations. Number of authors in the literature found the steady state response of non-oscillating moving load of an undamped foundation case [30-32]. They study the influence of moving load on an infinite supported beam with undamped springs. Mathews in his papers [27, 28], used Fourier transformation to calculate the solution for the steady-state vibration of damped and un damped Euler Bernoulli beam due to oscillating moving load. Duffy [33] calculated the solution of the combined responses of transit and steady state responses of a beam on elastic foundation under a moving oscillating load. The author transformed the differential equation of the system into space and time domains. Duffy used Fourier transformation to make the differential equation with respect to space and he used Laplace transformation to make it with respect to time. Fryba [34], studied in detail the models of finite and infinite beams under moving oscillating load. The author found the responses of different loading patterns moving on finite and infinite beams models.

Viscous damping is used in the above-mentioned papers, however Kim and Roesset [35] used linear hysteretic damping to investigate beam on elastic foundation under either constant amplitude or harmonic moving load. The authors used Fourier transformation methods in the study to find the response in the transformed field of domain. They look on the effects of velocity, damping, loaded length and load frequency on the deflected shape and maximum displacement.

Single discontinuous beam models

All of the above beam models are modelled as continuous models without discontinuity, however, there are variety of methods in the literature to solve discrete continuous models that take into accounts the dynamic behavior of the discontinuity of the rails along the track such as rail joints and discrete supports (sleepers) which are periodically applied in the presented models.

An in depth study of wave propagation in two coupled systems ; mono and multi coupled system has been done by Mead [36, 37]. In his papers, it is found that there are two types of zones found for the response of the structure as a function of frequency. Due to the periodicity, the two zones are observed. The two noticed zones are, stopping band zone at where the energy does not dissipate in the structure and passing band zone at where the energy propagate in the structure.

Jezequel [38] analyzed infinite beam supported periodically by lateral and torsional stiffness under non-oscillating moving loads by using the generalized Fourier method. Using this method facilitated the process of describing the behavior of all the points of the beam with respect to space and time in one deferential equation. The author summed a series of delta function that represent the periodical discontinuities. Solutions of the steady state are summed as a Fourier series with unknown coefficients that are found by substituting the solutions back to the differential equations of motion, then the equations are Fourier transformed into algebraic equations that can be solved for the unknown coefficients.

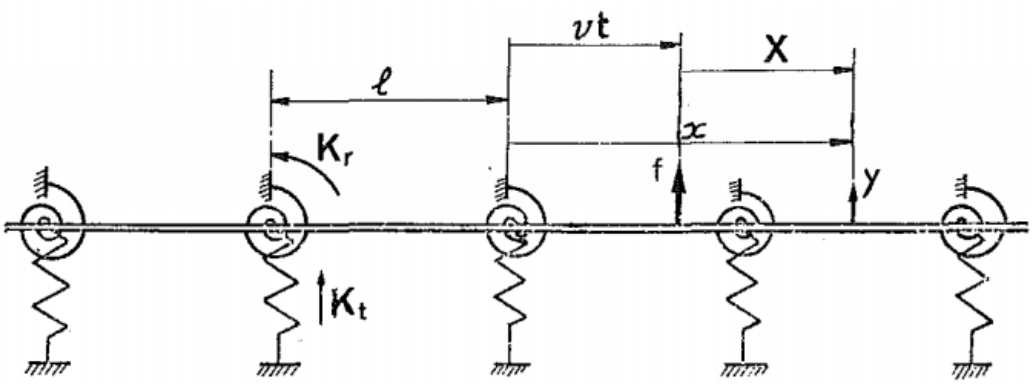

Figure 7: Beam in a periodic structure subjected to a moving force [38]

Kisilowski. et al. [39] did Jezequel's method taking into consideration the moving load on a periodically supported rail, where the load applied is the wheel load. The wheel is modelled as mass of single degree of freedom on a spring moving with zero acceleration. The same method was used to study disconnectedly supported rail under moving wheel set and harmonic moving load by Ilias and Muller [40]. Krzyzynski [41] modelled Euler Bernoulli infinite beam supported discretely using Floquet's method under a harmonic moving load. The discreet supports under the Euler Bernoulli Beam consist of spring dashpot to consider the rail pad, a mass to account for sleeper and one more spring dashpot to take into consideration the ballast. Krzyzynski used Floquet's solution of the differential equation of motion taking the benefit of the periodicity condition of the track in the longitudinal direction. Furthermore, he analyzed the wave propagated along the infinite Euler Bernoulli beam. Muller et al. [42] did a comparison between two semi analytical methods that are used in solving infinite periodic structures using two beam formulations to account for the rail. They apply Generalized Fourier method using Timoshenko beam theory and Floquet's methods using Euler Bernoulli beam. For Timoshenko beam, it was modelled with significantly

high shear stiffness, low damping and significantly low rotational inertia. The other beam formulation (Euler Bernoulli beam), was modelled as an un damped beam. The results were compared to the corresponding Timoshenko beam results and they found that the two methods produce similar results.

Hildebrand [43] investigated in the vibration reduction in railway tracks. His model includes the two rails supported by periodical sleepers on continuous visco-elastic foundation. The continuous visco-elastic foundation is used in his model to account for the ballast layer. His technique in his paper was based on considering a junction of the rail on the sleeper and computes the displacements. The calculated displacements were in terms of evanescent and propagating waves. Three groups of equation were taken into consideration in calculating the solution. The three set of equations are expressing: the compatibility conditions, the periodicity in the longitudinal direction and the reflection of waves from the junction on the other rail. Hildebrand found that at frequencies above 200 Hz, a model missing the second rail over calculates the attenuation. Another model of continuous discretely supported beam done by Nordborg [44] using Euler Bernoulli beam supported by different discrete supports. His model used to calculate a closed form solution under oscillating nonmoving load. The equations of motion used in his paper are transformed to wavenumber –frequency domain then solved using Floquet's method. In another paper [45] he used Green's function results [44] in the frequency- space domain to find the rail response under oscillating moving load. The author integrated in the space domain the Green's function multiplied by frequency domain force at specific frequency in order to find the frequency domain response at certain rail point. The author used this technique to study vibration from unevenness railway under moving wheel.

Smith and Wormley [46] use the Fourier transform techniques which is used to do computations for one repetitive unit and by using the periodicity condition the solutions for the other units are obtained. They used Fourier transform techniques to model a Euler Bernoulli beam periodically supported under a constant moving load. In computing the beam response under spatially distributed load the convolution integrals are used. They did an approximation representation model of the infinite span of the beam by modelling finite spans supported in a periodic manner. Regarding Fourier transform methods, differential equations of the selected unit (finite span) is transformed to frequency domain and an unknown coefficient resulted from this transformation are solved by using the boundary conditions of the unit. The resulted equations are then transformed to time domain. The periodicity condition is used to account for the infinite beam span. Smith et al. [47] In another paper used different technique called an approximate modal analysis technique. In this paper, they coupled vehicle model with the track by modelling a finite beam as an approximation of the infinite beam model.

Resilient hinges where used by Belotserkovskiy [48] to account for rail joints in his model. The author modeled the rails as a Euler Bernoulli beam under harmonic moving load. The author used Fourier transform techniques to study his model. The author used the same technique to analysis Timoshenko beam model with discontinuous supports.

Double beam models

Double beam models are mainly used to model slab tracks as the top beam is accounting for the rails and the bottom one is accounting for the slab. However, the literature does include many investigations on double beam system with one layer of resilient elements between the two beam layers.

For example Kessel [49] studied the resonance conditions in double beam system with an elastic layer in between under moving oscillating load. The double beam system used by Kassel is simply supported with finite length. The author found that in addition to the expected case of resonance- that happened when the frequency off the applied load corresponds to the natural frequency of the system- the load movement frequency also causes resonance of the system.

Vu et al. [50] Investigated the vibration of double beam system under harmonic excitation to find the complete solution. The resilient layer is representing the distributed visco elastic material. In his model Euler Bernoulli formulation with viscous damping are used. The differential equations are solved by changing variables and doing modal analysis. Han and Shiu [51] modelled an elevated railway track under a harmonic moving loads. They modelled an elevated ballast track for three different cases using Timoshenko beam formulations. Two of the presented cases in this paper are double beam models. One is modelled as finite simply supported double beam system with a visco-elastic layer in between representing the ballast.

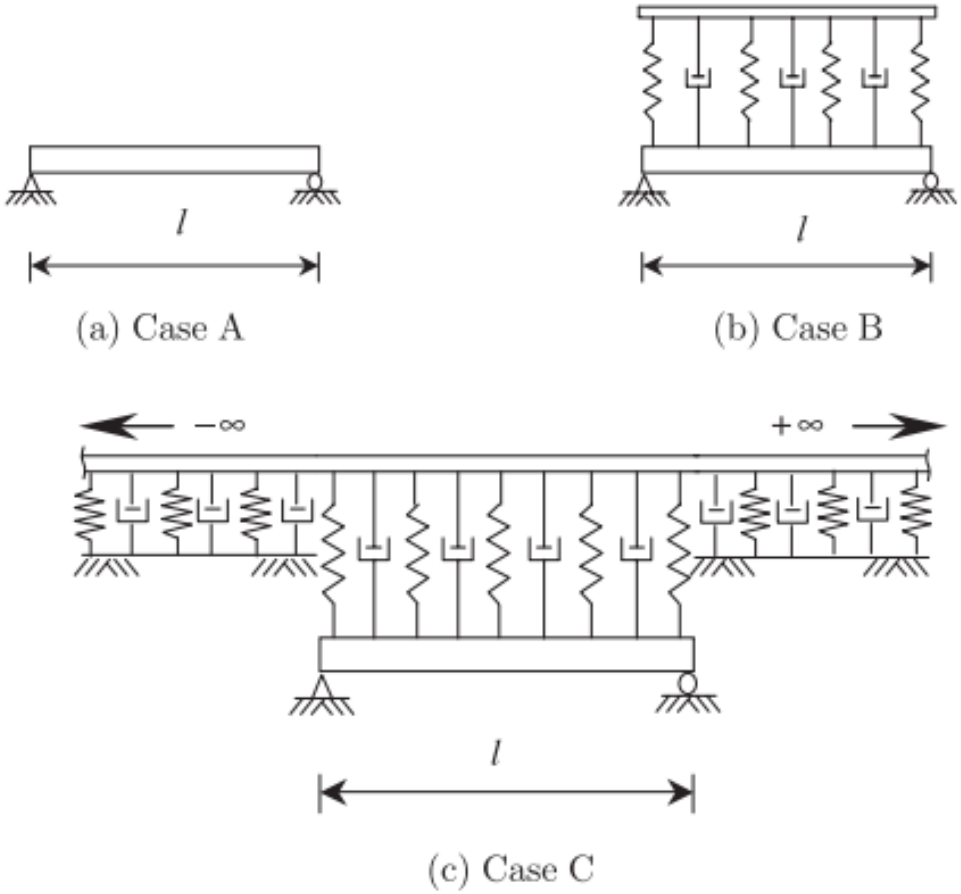

Figure 8: The models of an elevated railway used in [51]

In this model the top Timoshenko beam is accounting for the rails and the bottom on is accounting for the girder. The other one, is taking into account the fact of track infinity. They model it as a semi-infinite structure on the left and right side of the elevated model. The semi-infinite section is modelled as Timoshenko beam on a visco-elastic foundation. This paper came out with the resonant curves for the three cases of an elevated railway tracks under moving harmonic loads.

Floating Slab Track

In the floating slab tracks the concrete slab is supporting the rails via the fastening system and rail pads and is setting on the slab bearings. This part of the track (concrete slab) can be discontinuous slab units or continuous slab. If the concrete is poured in situ it will be continuous floating slab track. However, if it is precast concrete units, it will be discontinuous floating slab track.

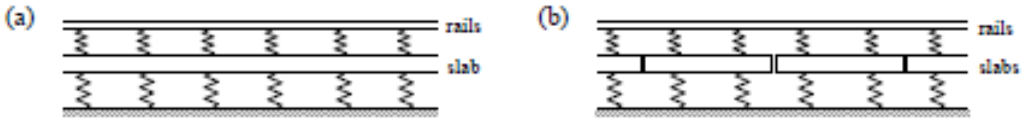

Figure 9: Double-beam models of floating-slab track with (a) a continuous slab (cast in-situ) and (b) discrete slabs (pre-cast sections) [52]

Samavedam and Cross [53] modeled floating slab track to investigate vibration isolation. They used two Winkler beam representing rails and slab. First beam that represent rails, is setting on a mass of springs that account for the rail pads supported by the second beam that account for the concrete slab part of the track. Slab beam is resting on a mass of springs that account for resilient elements. In their model they deal with the tunnel floor as a rigid foundation. Forrest [52] modeled continuous and discontinuous floating slab tracks under oscillating nonmoving load using repeating unit method. In his model the rails and slab are modelled as infinite Euler Bernoulli beams. For the slab beam the author used an infinite homogenous beam to account for continuous floating slab tracks. For discontinues floating slab tracks, he used finite slab beams periodically supported by resilient bearings springs. Forrest used Dynamic

Stiffness method with Repeating Unit method to report the relationship between deformation and forces on the left and on the right of the repeating units. Then the Dynamic Stiffness matrix of the semi-infinite track (on the left or right of the load) is produced using Floquet's method. Using the boundary condition of the semi-infinite track and the fact of that at infinity the responses decay to zero the track response can be obtained.

Cui and Chew [54] used Receptance method to investigate the effectiveness of floating slab track to fixed slab track system under moving and non-moving harmonic loads. Floating slab track in this paper, is modelled as double Timoshenko beams. For the slab part in the model, it is modeled discontinuously supported elastically by continuous elastic foundation. In solving the differential equations of motion, they used Laplace transformation techniques. When it is compared to the fixed slab track, they found that floating slab tracks reduce the forces transmission for frequencies above designed frequency.

Hussein and Hunt [55] extend Forrest's continuous floating slab model with accounting for oscillating moving loads. They used two Euler Bernoulli beams to account for the rails and the slab and two layers of s continuous springs. The first layer is to account for rail pads that are between rails and the slab. The second layer is used to represent the slab bearings below the slab. They used Fourier transformation method to compute displacements of the track. They also include in this paper a brief explanation of basic concepts of vibration of infinite systems. In another paper Hussein and Hunt [56] used different methods to model discontinous floating slab track under moving oscilliating load. The authors used three methods of modelling the discontinous floaing slab track. The three methods used are: Repating Unit method, the Periodic Forier method and the Modified Phase method. The authors found out that velocitices

less than 100 Km/hr has an insignificant effect on the displacment of the floating slab track. In another paper [57], they modelled discontinous floating slab track to study the dynamic effect of slab discontinuity in the underground railway on the running trains. The authors used Fourier series techniques to develop a method to couple moving train to a discontinous floating slab track.It is found that dynamic behaviour due to slab discountuinty is affected if the heavy trains or high speed trains are running in the underground railway tracks.

Hussein and Costa [58] accounts for discontinuous floating slab tracks with end bearings and they study its dynamic behavior. They used the same model of discontinues floating slab track mentioned in the previous works. They applied an end bearing between discontinuous slab units under harmonic moving load. They aimed to explain the effect of the vertical stiffness of the end bearings on the dynamic response of the tracks. They found that, the use of the end bearings between discountinous slab units reduce vibraton at free-free slb reasonance.

Yang et al. [59] applied stiffness Enhancement Measure (SEM) of slab end for discontinuous FST. They coupled dynamic model for train and FST to investigate the dynamic behavior of SEM on the train and FST. SEM can be done by increasing the supporting stiffness at the slabs ends and/or applying of end slab bearings between consecutive slab units. They studied the dynamic influence of each SEM on the train and FST. In their paper they determined optimal parameters for both SEMs to be used in the design of FST. They found that SEM at positions of slab ends has considerable significance on dynamic behaviors of FST. Elsewhere in the trach it has negligible effect. Also, using end bearings allow to increase service life of fasteners as it improves loading condition of fasteners at slab ends. Vertical displacement is significantly reduced by applying supportive stiffens at slab ends.

Wei et al. [60] used dowel joints in their discountinous FST model and explore its influence on the dynamic behaviour of train-FST system. The authors used two dowel models to model dowel joints at the ends of discountinous FST. The two dowel joints models are shear spring dashpot model and bending spring dashpot model.For the vertical restrictions, shear spring dashpot model is appplied and for rotatinal restrictions bending spring dashpot model is used. The authors used modal superpoition method and Newtmark β method to numerically calaculate the results. The authors did a prarmetric analysis for three cases including no dowel model,shear dowel model and bending dowel model. The authors found out that vibration is reduced by using both shear and bending dowel models. The displacement difference of adjacent FS is reduced significantly in shear dowel model with out decreasing displacment amplititude.Where, it is the opposite for bending dowel model. The stiffness of the both dowel model influence significantly the analysis for train-FST system, where damping coffecitns have almost negligble effect.

2.3 Experimental Vibration Measurements

A experimental vibration measurements provide a valuable data of vibrations induced by running trains. Number of researchers measured vibrations from an in situ FSTs; and Others have conducted vibration tests on FSTs prototypes in a laboratory environment. This section reviews the in-situ and laboratory vibration tests conducted on different FSTs systems.

2.3.1 In Site Vibration Measurements

The earliest in situ vibration measurements were done by Rücker in 1977 [61]. The author measured induced vibrations for Berlin Metro. London Transport Office of the scientific adviser measured vibrations of Jubilee line of London underground railway at Baker Street on 1982 [62].

In 1990,vibration measurement data was collected from Beijing subway railway tunnel at pre-located points of the track [63]. The measurements are used to analyze dynamic responses of specified points on the track under moving train.

Wolf measured induced vibration from underground light rail transit [64]. The author aimed to anticipate ground vibration at low frequencies. In his work, he showed results of predictable ground displacement of nearby structures from underground light rail transit operations using experimental measurements and finite model.

From on ground and in underground level vibration measurement were obtained from underground tunnel of Line 1 of the Beijing Mero in China [65].

San Francisco Bay Area Rapid Transit (BART) system experienced many vibration measurements [11]. The data was collected from different forms of the Bay area rapid transit system. The different forms includes : resiliently supported half-sleepers ,floating slabs and high-resilience fasteners in subway and section of floating slab used on ground level track. The work aimed to anticipate future vibration mitigation from the track. The results showed that some of the track forms used in BART system produced as expected results of vibrations like floating slabs and high resilience fasteners. The results of high resilience supported half-sleepers were not promising as expected.

The Bakerloo line of London Underground experienced an in-situ vibration tests [66]. The tests were within the CONVURT project at a location in Regent's Park. A test train is used to do the vibration measurements. It passed 35 passages during the experimental tests with a speed range of 20km/h to 50km/h. Vibrations were conducted on the test train's axel box, on the tunnel wall and tunnel invert and on different levels of the ground. For the ground vibration data, the data was collected on the ground level and 15 m below the ground level. Two buildings were used two conduct vibrations from

floors and columns of the structures. The buildings were 70 m away from the tunnel. The collected data assisted to determine the dynamic soil properties, rail and wheel roughness and track properties.

2.3.2 Laboratory Vibration Measurements

At an underground laboratory of Beijing Jiaotong University a low frequency vibration measurements were carried out on floating slab track[67]. SBZ30 unbalanced shaker was used as low frequency experiment excitation source (Figure 10). Vibration responses were collected from bogie of the shaker, the slab, the rail, the tunnel invert and apex. A distance of 80 m from the track and on nearby many floors building, the measurements were also obtained.

Figure 10: Unbalanced shaker used in the experiment [67].

The results of the experimental vibration test aimed to improve methods of controlling low frequency vibrations. The collected data can be used to develop efficient countermeasures to reduce low frequency vibration mitigation.

An innovative floating slab track was used to reduce amount of vibration by implementing recycled rubbers as slab bearings [68]. An experimental test was carried out to investigate dynamic and static behavior of the railway track. The test has done on the floating slab track prototype of ISOLGOMMA Research Centre in Pozzuoli (Figure 11). The experimental results are then used to validate numerical model. The numerical model is used to investigate different configuration of the innovative bearing system with different mechanical characteristics of the recycled rubber.

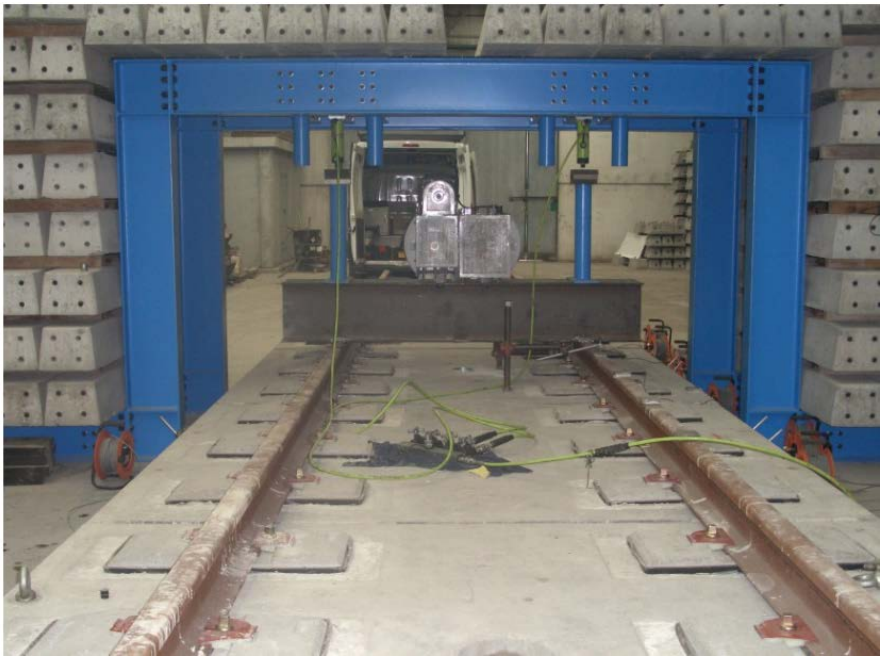

Figure 11: FST prototype used in the experimental measurement [68].

In 2015 many laboratory tests carried out on floating slab track with different bearing forms. The experimental measurements were conducted at underground laboratory of Beijing Jiaotong University [69]. Bearing supporting forms used under the floating slab track in the test were: linear supporting (Figure 12), full-surface supporting and point supporting (Figure 13).

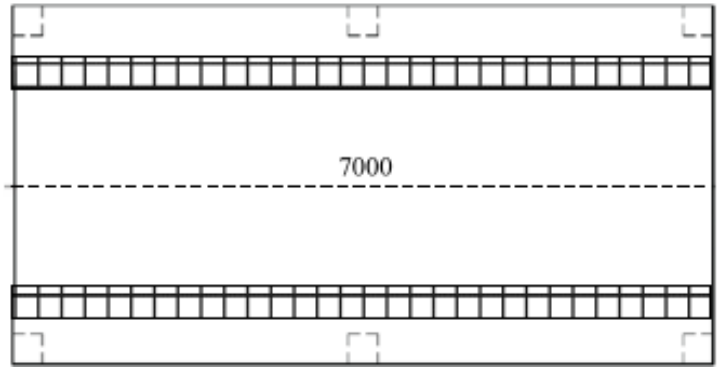

Figure 12: Plan view of the FST with linear supporting form used in the test [69]

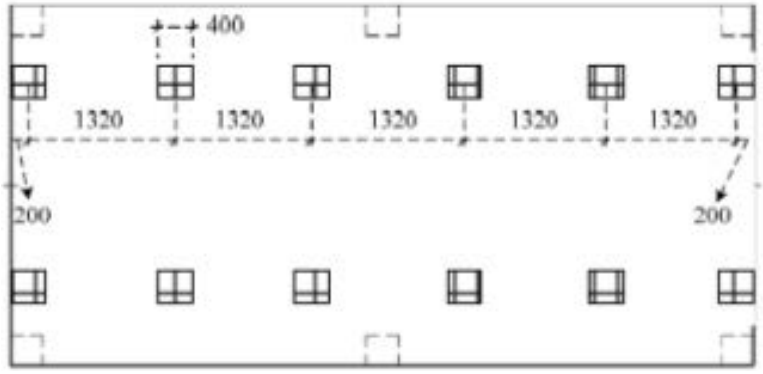

Figure 13: Plan view of the FST with point supporting form used in the test [69].

Using frequency spectrum and time history analysis they found that the first resonant frequency of the point supporting, and linear supporting forms is less than the full surface supporting form. This difference is because of the declining supporting stiffness beneath the track. This reason illustrated the behavior of having an increase in the peak values of vibration accelerating in the frequency domain and time domain for floating slab track with point supporting and linear supporting forms. Floating slab track with point bearing supporting form has the lowest transfer ratio of vibration from the slab to the tunnel.

An innovative integration between floating slab track and dynamic vibration absorbers (DVAs) to form vibration attenuation track (VAT) was tested experimentally[70].VAT passed through experimental tests and theoretical model to verify it's capability of mitigating vibration at low frequencies.

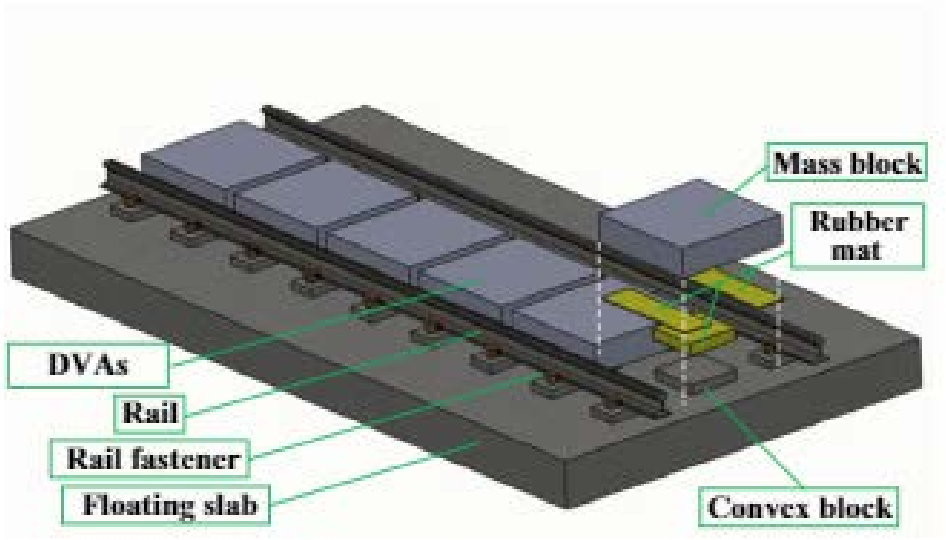

Figure 14: Proposed vibration attenuation track [70].

The parameters of VAT that include dynamic vibration absorbers with floating slab track are determined from theoretical model (Figure 15) by using modal analysis technique and fixed-point theory.

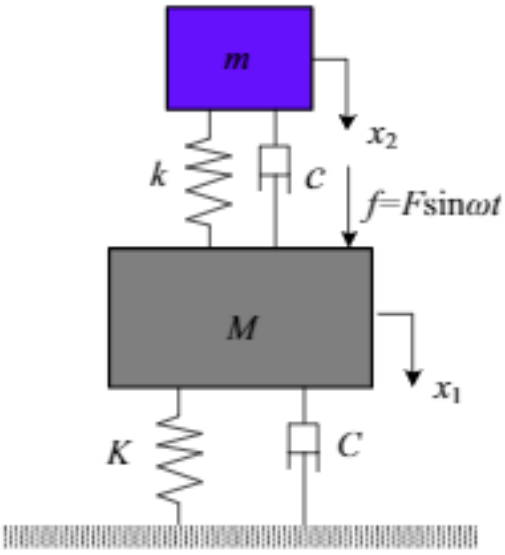

Figure 15: Single degree of freedom system attached with a DVA [70].

The vibration reduction behavior of the VAT is studied under train dynamic excitations using three-dimensional model coupling train with VAT system. The coupled three-dimensional model is validated by experimental measurements on full scale VAT prototype (Figure 17) under different harmonic excitations.

Figure 16: Full scale VAT prototype [70].

Both experimental and computational results show that DVAs absorb vibrations effectively. This absorption of vibration helps in significantly reducing subgrade vibrations at low frequencies. In site experiment on elevated Hangzhou Metro Line 1 railway track has been carried out in 2018 to experiment ways of minimizing noise from metro viaduct [71]. In their work, three test cases were measured: using noise barrier with rack bed, using noise barrier with elastic mat FST and full surrounded noise barrier 5.1 m length with elastic mat FST. The three situations used in the test are shown in Figure 17.

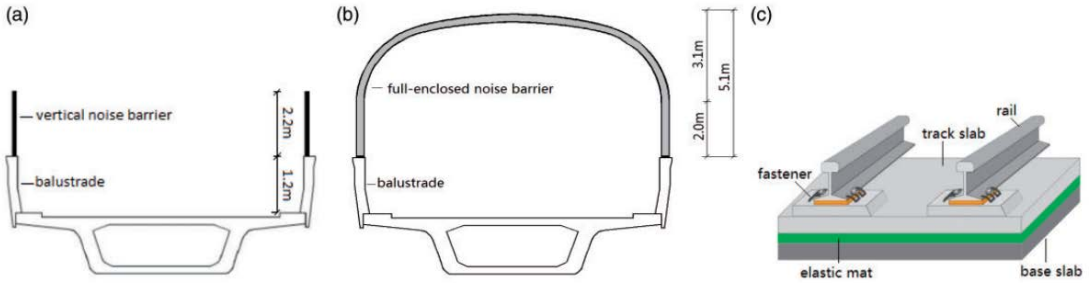

Figure 17: The applied situations for the experiment: (a) using noise barrier, (b) 5.1 m full surrounded noise barrier, (c) elastic mat floating slab track [71].

The data was collected from the measuring points on the rails, the bridge and on the ground. The data was analyzed to see the reduction of noise from metro viaduct using different way of implementing noise barrier and elastic mat. The results of using elastic mat show an effective decrease of transferring vibration coming from wheel rail interaction to the bridge, but it could increase wheel rail noise. When elastic mat is tested the noise, reduction was noticed to be excellent on ground and in the region bottom of the bridge. For the measuring points in the region above and near to the rails a noticeable increase in noise has been detected. For bridge born noise there were no difference of reducing noise between two kind of noise barriers (vertical and full enclosed noise barriers). The full enclosed noise barrier reduces the noise coming from wheel rail interaction more than vertical noise barrier.

2.4 Gap of Knowledge

As presented in the literature above extensive analytical and experimental investigations have been conducted for both continuous and discontinuous FSTs. Obviously, the previous numerical models cannot be used to investigate the dynamic behavior of the special FST which a constant cross-section assume along each slab unit. Furthermore, the actual behavior -that can be obtained by experimental measurements- of the special FST is not provided in the previous reported experimental investigations.

2.5 Thesis Novelty

In this thesis, the previous numerical models of FST is going to be modified to take into consideration the existence of the periodic grooves along the slab. The model is going to account for the changing cross sections of each slab unit. Dynamic behavior of this special FST model is going to be investigated under harmonic non-moving excitation in both bending and torsion. Besides, the special type of FST is going to be investigated experimentally by an in-situ vibration tests on a full-scale finite length mock up structure representing the special FST.

2.6 Thesis Objectives

As mentioned in Section 1.3, the aim of this work is to explore the influence of changing the groove thickness on the dynamic behavior of the special infinite FST. To do so, the infinite continuous FST model proposed in [52] is modified taking into account the changed cross sections of the slab unit -due to the existence of the periodic groove in the slab unit- along the track. A full-scale mockup structure of the special FST with finite length is used for numerical and experimental investigations. For the numerical investigations, a fast running model based on the Dynamic Stiffness method and three-dimensional FE model are created where, the research assistant developed the FE model. The vibration response of the fast running model is then compared with

responses obtained from FE model for verifying the both numerical models. For the experimental investigations, an impact test is performed to identify the actual transfer functions of the mockup structure and to validate the fast running model. Then, the fast running model initial parameters are fine-tuned through model updating procedures done by the research assistant. The updated model is utilized in a parametric study to evaluate the influence of varying the thickness of the grooves on the dynamic response of the infinite special FST. The work carried out in this thesis is summarized in Figure 18.

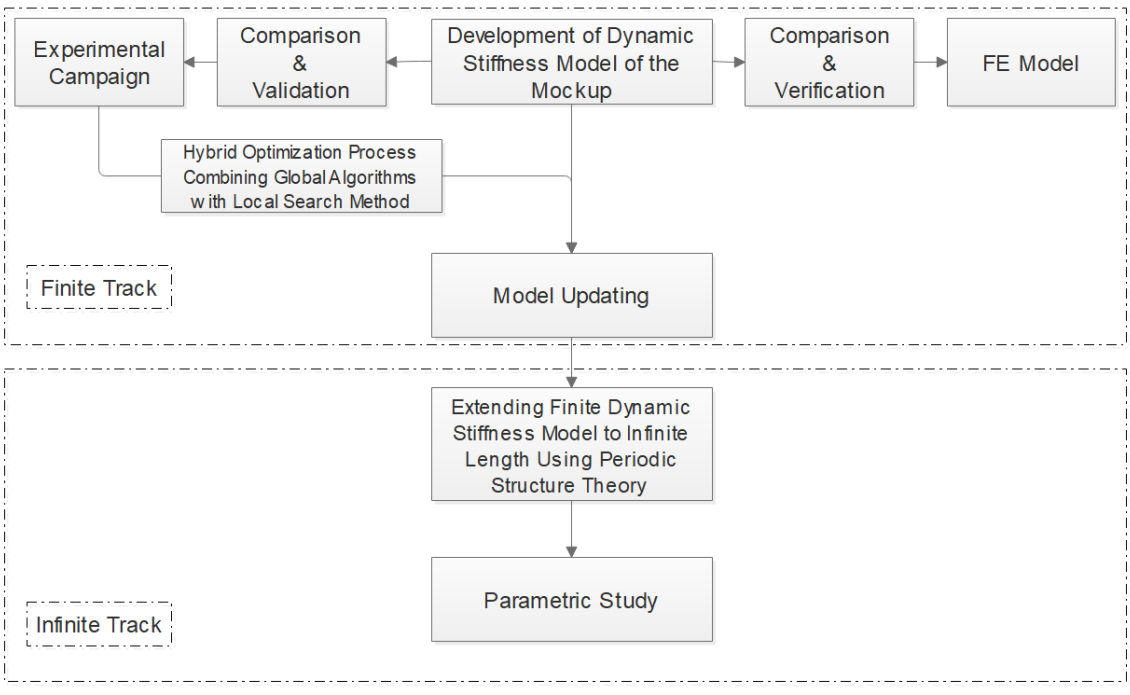

Figure 18:Flow chart of the work of this thesis.

CHAPTER 3:MODELS' FORMULATION

3.1 Introduction

In this chapter a fast running model based on the Dynamic Stiffness Method and a three-dimensional FE model are developed to model the special FST.

For the fast running model, the model presented in [52] is modified to account for the cross sections variations along the slab units. The formulation of the fast running model includes the following subsections. The formulation of the equations of motion that describe the bending and torsional behavior of the track. Also, the computational process of the Dynamic Stiffness Matrix using Dynamic Stiffness Method. Then the development of the finite model of the special FST. Finally, the formulation of the infinite case of the special FST using Floquet's Theorem.

The FE model of the special FST, Abaqus 6.14 FE software [72] is used to develop the Three Dimensional (3D) FE model. The FE model formulation section in this chapter defines the characteristics used in the Abaqus 6.14 FE software that is operated to develop the 3D FE model.

Furthermore, the multi-unit mockup structure representing the special FST is described at the beginning of this chapter, as its features are going to be used in the fast running model of the mockup and in the FE model for the verification process that is carried out in Chapter 4. The case of infinite special FST is going to be used in the parametric study shown in Chapter 5.

3.2 The Mockup Track

The authors were given access to a full-scale mockup structure that represents the special FST system used in Doha metro. As shown in Figure 19, the mockup FST consists of 4 precast slab unit resting on heavy mass concrete. The floating slab is supported on 24 rubber point bearings distributed along the track underneath the heavy mass concrete. The precast slab units are 4.1-m-long spaced at 0.1 m intervals resulting in a total track length of 16.7m. The rails were attached to the precast slabs at 0.7 m intervals using 24 fasteners per rail.

As depicted in Figure 20, four cross-sections with different geometries can be found along the floating concrete slab:

Cross Section 1: precast slab unit and heavy mass concrete with shoulders.

Cross Section 2: precast slab unit and heavy mass concrete without shoulders.

Cross Section 3: heavy mass concrete only.

Cross Section 4: heavy mass concrete with shoulders.

Figure 19: The mockup FST.

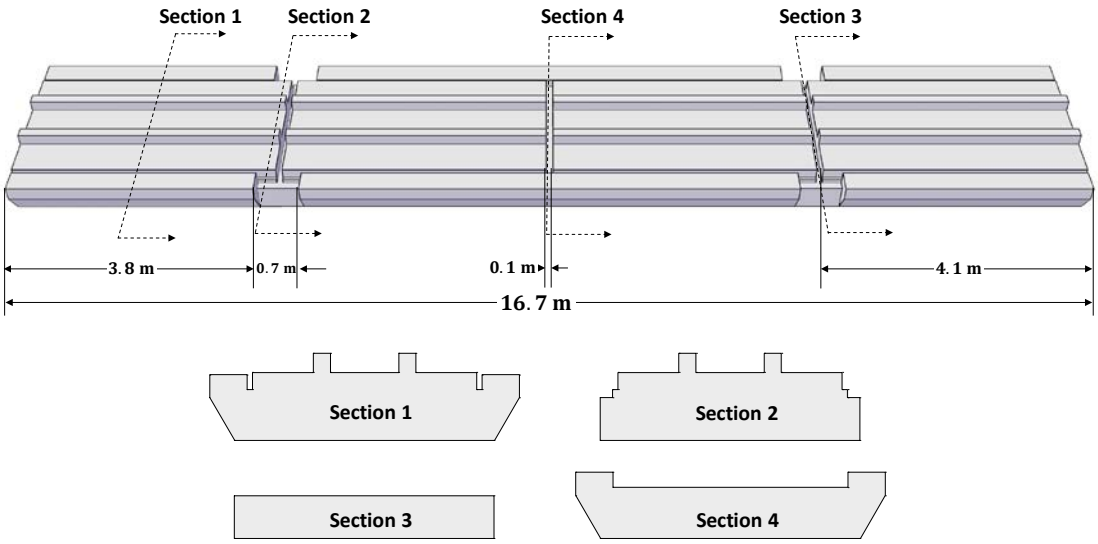

Figure 20: Dimensions and cross-sections of the concrete slab of the mockup track.

3.3 The Fast Running Model Formulation

Modeling the special FST utilizing Periodic Structure theory, improves understanding of its dynamic behavior with less computational time compared to the FE model. As illustrated in Figure 21, the model is consisting of three Euler Bernoulli beams. The upper two beams are representing the rails. The lower one is representing the slab part of the track. The slab part of the track consist of two segments to account for the changing of the slab cross sections. There are four continuous elastic layers (springs and dashpots) representing rail pads and slab bearings. The Track is resting on a rigid foundation. In this section special FST is going to be modelled using Dynamic Stiffness Method for a non moving concetrated harmonic load applied on the rails. The slab is modelled in both bending and torsion. The whole track is divided into number elements and the Dynamic Sifness Matrix (DSM) is going to be computed for each element.

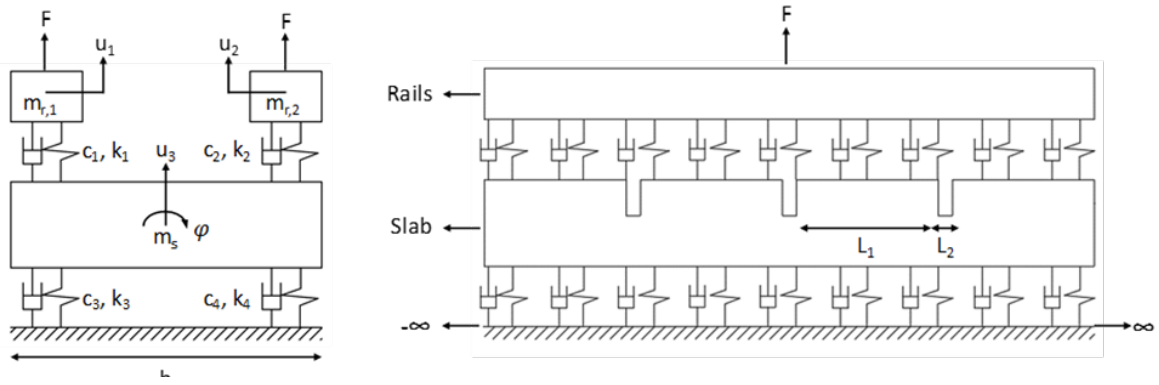

Figure 21: Illustration of the model. (a) Cross section view. (b) Side view.

3.3.1 Equations of Motion

To start modelling the special FST, it is necessarily to know the equations of motion for a beam subjected to bending and torsion. For Euler Bernoulli beam the convention formula for bending and torsion are as the following[73]:

For bending

$$EI\frac{\partial u^4}{\partial x^4} + m\frac{\partial U^2}{\partial t^2} = f(x,t) \tag{1}$$

where EI is the flexural stiffness of the beam (E is the Young's modulus, I is the Moment of Inertia), u is the vertical displacment, m is the mass of the beam per unit length and $f(x,t)$ is the external applied force per unit length of the beam.

For torsion

$$J\frac{\partial \varphi^2}{\partial t^2} - GK\frac{\partial \varphi^2}{\partial x^2} = \tau(x,t) \tag{2}$$

where J is the polar mass moment of inertia per unit length, φ is the angle of twist, GK is the torsional stifness of the beam (G is the Shear Modulus, K the Torsion Constant of the cross section) and $\tau(x,t)$ is the external applied torque per unit length.

Applying the conventional bending and torsional equations for Euler-Bernoulli beam on the beams of the special FST model as shown in Figure 21 obtain the following equations:

For the left rail, the governing bending equation is

$$EI_{r,1}\frac{\partial {u_1}^4}{\partial x^4} + m_{r,1}\frac{\partial {u_1}^2}{\partial t^2} = f(x,t)_1 \tag{3}$$

where

$$f(x,t)_1 = -K_1\left(u_1 - \left(u_3 + \varphi\frac{b}{2}\right)\right) - C_1\left(\frac{\partial u_1}{\partial t} - \frac{\partial(u_3 + \varphi\frac{b}{2})}{\partial t}\right) \tag{3.1}$$

For the right rail, the governing bending equation is

$$EI_{\mathrm{r},2}\frac{\partial {u_2}^4}{\partial x^4}+m_{\mathrm{r},2}\frac{\partial {u_2}^2}{\partial t^2}=f(x,t)_2 \tag{4}$$

where

$$f(x,t)_2=\ -K_2\left(u_2-\left(u_3-\varphi\frac{b}{2}\right)\right)-C_1\left(\frac{\partial u_2}{\partial t}-\frac{\partial(u_3-\varphi\frac{b}{2})}{\partial t}\right) \tag{4.1}$$

For the slab there are two governing equations. One for bending and the other one is for torsion. For the bending, the slab governing bending equation is

$$EI_3\frac{\partial {u_3}^4}{\partial x^4}+m_3\frac{\partial {u_3}^2}{\partial t^2}=f(x,t)_3 \tag{5}$$

where

$$f(x,t)_3=$$

$$K_1\left(u_1-\left(u_3+\varphi\frac{b}{2}\right)\right)+C_1\left(\frac{\partial u_1}{\partial t}-\frac{\partial(u_3+\varphi\frac{b}{2})}{\partial t}\right)+K_2\left(u_2-\left(u_3-\varphi\frac{b}{2}\right)\right)$$

$$+C_2\left(\frac{\partial u_2}{\partial t}-\frac{\partial(u_3-\varphi\frac{b}{2})}{\partial t}\right)-K_3\left(u_3+\varphi\frac{b}{2}\right)-C_3\frac{\partial(u_3+\varphi\frac{b}{2})}{\partial t}-K_4\left(u_3-\varphi\frac{b}{2}\right)$$

$$-C_4\frac{\partial(u_3-\varphi\frac{b}{2})}{\partial t} \tag{5.1}$$

For the torsion, the slab governing torsion equation is

$$J_3\frac{\partial\varphi^2}{\partial t^2}-GK_3\frac{\partial\varphi^2}{\partial x^2}=\tau(x,t)_{\ 3} \tag{6}$$

where

$$\tau(x,t)_3 =$$

$$-\frac{b}{2}\left[K_3\left(u_3+\varphi\frac{b}{2}\right)-K_4\left(u_3-\varphi\frac{b}{2}\right)-K_1\left(u_1-\left(u_3+\varphi\frac{b}{2}\right)\right)\right.$$

$$\left.+K_2\left(u_2-\left(u_3-\varphi\frac{b}{2}\right)\right)\right]-\frac{b}{2}\left[C_3\frac{\partial(u_3+\varphi\frac{b}{2})}{\partial t}-C_4\frac{\partial(u_3-\varphi\frac{b}{2})}{\partial t}\right.$$

$$\left.-C_1\left(\frac{\partial u_1}{\partial t}-\frac{\partial(u_3+\varphi\frac{b}{2})}{\partial t}\right)\quad+C_2\left(\frac{\partial u_2}{\partial t}-\frac{\partial(u_3-\varphi\frac{b}{2})}{\partial t}\right)\right] \qquad (6.1)$$

The general solution for bending equations (3), (4) and (5) in time and space domain is as the following:

$$U=\begin{bmatrix}u1\\u2\\u3\end{bmatrix}e^{i(\omega t+\xi x)} \qquad (7)$$

for the general solution for torsion equation (6) in time and space is as the following

$$\varphi=\phi e^{i(\omega t+\xi x)} \qquad (8)$$

substituting the general solution in the equations (3), (4), (5) and (6) and equalize it to zero, results in the following matrix (next page).

The below matrix can be simplified to be written as

$$[A]\begin{bmatrix}u1\\u2\\u3\\\phi\end{bmatrix}=0 \qquad (9)$$

where, equation (9) has two possible solutions:

1. Trivial solution.
2. Non-trivial solution.

$$\begin{bmatrix} EI_{r,1}\xi^4 - m_{r,1}\omega^2 + i\omega C_1 + K_1 & 0 & -i\omega C_1 - K_1 & \frac{b}{2}[-i\omega C_1 - K_1] \\ 0 & EI_{r,2}\xi^4 - m_{r,2}\omega^2 + i\omega C_2 + K_2 & -i\omega C_2 - K_2 & \frac{b}{2}[i\omega C_2 + K_2] \\ -i\omega C_1 - K_1 & -i\omega C_2 - K_2 & \begin{matrix} EI_3\xi^4 - m_3\omega^2 \\ +i\omega C_3 + K_3 \\ +i\omega C_4 + K_4 \\ +i\omega C_1 + K_1 \\ +i\omega C_2 + K_2 \end{matrix} & \frac{b}{2}\begin{bmatrix} i\omega C_3 + K_3 \\ -i\omega C_4 - K_4 \\ +i\omega C_1 + K_1 \\ -i\omega C_2 - K_2 \end{bmatrix} \\ \frac{b}{2}[-i\omega C_1 - K_1] & \frac{b}{2}[i\omega C_2 + K_2] & \frac{b}{2}\begin{bmatrix} i\omega C_3 + K_3 \\ -i\omega C_4 - K_4 \\ +i\omega C_1 + K_1 \\ -i\omega C_2 - K_2 \end{bmatrix} & \begin{matrix} \frac{b^2}{4}\begin{bmatrix} i\omega C_3 + K_3 \\ i\omega C_4 + K_4 \\ i\omega C_1 + K_1 \\ i\omega C_2 + K_2 \end{bmatrix} \\ -J_3\omega^2 + GK_3\xi^2 \end{matrix} \end{bmatrix} \begin{bmatrix} u1 \\ u2 \\ u3 \\ \phi \end{bmatrix} = 0.$$

For the trivial solution, the matrix of $\begin{bmatrix} u1 \\ u2 \\ u3 \\ \phi \end{bmatrix} = 0$, in this case this means that there are no displacement responses for the rails and slab. This solution is rejected as it not the appropriate solution for our case.

For the non-trivial solution, determinant of $[A]$ is equal to zero. This solution is going to be handled to find the general solution expression. The general solution expression is presented below in the coming section.

Determinant of $[A]$ is a function of ξ, ω and prescribed track parameters : $EI_{\mathrm{r},1}, EI_{\mathrm{r},2}, EI_{3,}m_{\mathrm{r},1}, m_{\mathrm{r},2}, m_3, K_1, K_2, K_3, C_1, C_2, C_3, C_4, C_3, GK_3 \; and \; J_3$. The equation is of the 14th order. This means that, there are fourteen values of ξ. The excitation frequency ($\overline{\omega}$) must be equal to angular frequency. This equalization will satisfy the boundary conditions of the track under the load when it is divided into two semi-infinite tracks.

3.3.2 Computation of The Dynamic Stiffness Matrix

The track is divided into many elements. For each element the Dynamic Stiffness Matrix (DSM) is obtained. DSM is obtained for each element using the general solution expression for the response vector and boundary conditions of the element.

The general solution expression is

$$U = B_1 V_1 e^{\xi_1 x} + B_2 V_2 e^{\xi_2 x} + \cdots + B_{14} V_{14} e^{\xi_{14} x} \tag{10}$$

where, $U = \begin{bmatrix} u1 \\ u2 \\ u3 \\ \phi \end{bmatrix}$ is the response vector, $B_1, \ldots, B_{14}$ are the constant coefficients and V is the eigenvector values of the matrix A with zero eigenvalue, where for each value of ξ there is a corresponding vector of V; and this because the matrix A is already singular whenever the values of ξ is substituted.

The general solution equation is used to write the Dynamic Stiffness Matrix for single element using boundary conditions of the element. As illustrated in Figure22 and Figure 23, for a general element of the special FST, the left and right forces and displacements are:

$$Q_{1L}, Q_{2L}, Q_{3L}, M_{1L}, M_{2L}, M_{3L}, T_{3L}, u_{1L}, u_{2L}, u_{3L}, \theta_{1L}, \theta_{2L}, \theta_{3L}, \varphi_{3L}$$

$$Q_{1R}, Q_{2R}, Q_{3R}, M_{1R}, M_{2R}, M_{3R}, T_{3R,} u_{1R}, u_{2R}, u_{3R}, \theta_{1R}, \theta_{2R}, \theta_{3R}, \varphi_{3R}$$

where Q is the shear force, M is the moment, T is the torque, u is the vertical displacement, θ is the rotation angle and φ is the twist angle. Subscripts 1,2,3 represents the left rail, the right rail and the slab respectively. Subscripts L and R represents the left and right hand-side of the special FST element.

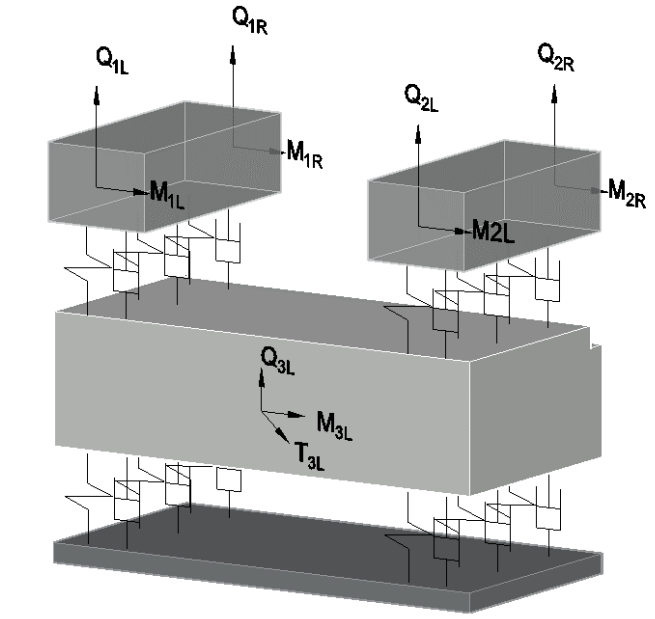

Figure 22: Boundry forces of an element of the specail FST (Right hand role is used to represent moment and torque).

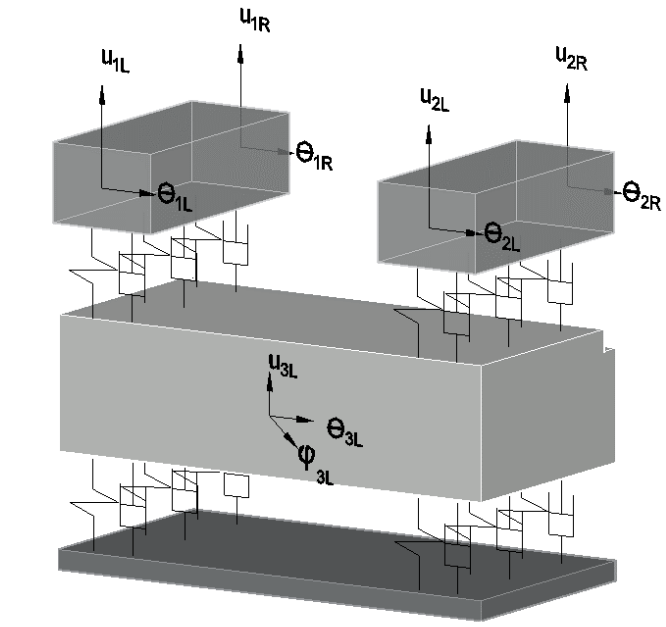

Figure 23: Boundary displacements of an element of the special FST (Right hand role is used to represent angle of rotation and angle of twist).

The special FST element as shown in Figure 22 or 23 is divided into two sub elements to account for the groove. In other words, the two sub elements have different slab segment's characteristics and similar rail characteristics as illustrated in Figure 24. DSM is going to be obtained for the sub elements and then by using joint boundary condition between two sub elements, the DSM for the whole element is computed.

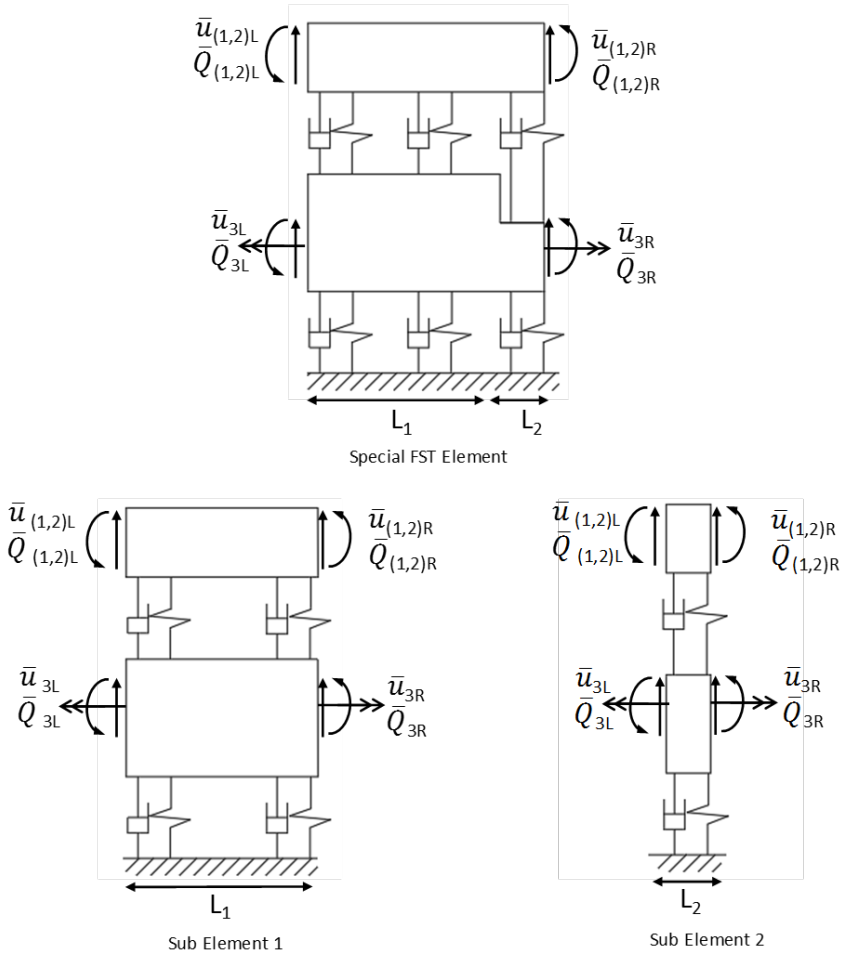

Figure 24: Boundary conditions of the special FST element and its two sub-elements (Side view).

The bar is used in Figure 24 to represent the condensed boundary conditions. Where $\bar{Q}$ is including shear force, moment and torque (for the slab beam). The $\bar{u}$ is including vertical displacements, rotation angle and twist angle (for the slab beam) at the ends of the element. The boundary conditions for the sub elements are shown in the following tables.

Table 1: Boundry Conditions of Sub Element 1

At $L_1=0$		At $L_1=L_1$	
$u1 = u_{1L}$	$EI_1 \frac{du1^3}{dx^3} = Q_{1L}$	$u1 = u_{1R}$	$EI_1 \frac{du1^3}{dx^3} = -Q_{1R}$
$\frac{du1}{dx} = \theta_{1L}$	$EI_1 \frac{du1^2}{dx^2} = -M_{1L}$	$\frac{du1}{dx} = \theta_{1R}$	$EI_1 \frac{du1^2}{dx^2} = M_{1R}$
$u2 = u_{2L}$	$EI_2 \frac{du2^3}{dx^3} = Q_{2L}$	$u2 = u_{2R}$	$EI_2 \frac{du2^3}{dx^3} = -Q_{2R}$
$\frac{du2}{dx} = \theta_{2L}$	$EI_2 \frac{du2^2}{dx^2} = -M_{2L}$	$\frac{du2}{dx} = \theta_{2R}$	$EI_2 \frac{du2^2}{dx^2} = M_{2R}$
$u3 = u_{3L}$	$EI_3 \frac{du3^3}{dx^3} = Q_{3L}$	$u3 = u_{3R}$	$EI_3 \frac{du3^3}{dx^3} = -Q_{3R}$
$\frac{du3}{dx} = \theta_{3L}$	$EI_3 \frac{du3^2}{dx^2} = -M_{3L}$	$\frac{du3}{dx} = \theta_{3R}$	$EI_3 \frac{du3^2}{dx^2} = M_{3R}$
$\phi = \phi_{3L}$	$GK \frac{d\phi}{dx} = -T_{3L}$	$\phi = \phi_{3R}$	$GK \frac{d\phi}{dx} = T_{3R}$

Table 2: Boundry Conditions of Sub Element 2

At $L_2=0$		At $L_2=L_2$	
$u1 = u_{1L}$	$EI_1 \frac{du1^3}{dx^3} = Q_{1L}$	$u1 = u_{1R}$	$EI_1 \frac{du1^3}{dx^3} = -Q_{1R}$
$\frac{du1}{dx} = \theta_{1L}$	$EI_1 \frac{du1^2}{dx^2} = -M_{1L}$	$\frac{du1}{dx} = \theta_{1R}$	$EI_1 \frac{du1^2}{dx^2} = M_{1R}$
$u2 = u_{2L}$	$EI_2 \frac{du2^3}{dx^3} = Q_{2L}$	$u2 = u_{2R}$	$EI_2 \frac{du2^3}{dx^3} = -Q_{2R}$
$\frac{du2}{dx} = \theta_{2L}$	$EI_2 \frac{du2^2}{dx^2} = -M_{2L}$	$\frac{du2}{dx} = \theta_{2R}$	$EI_2 \frac{du2^2}{dx^2} = M_{2R}$
$u3 = u_{3L}$	$EI_3 \frac{du3^3}{dx^3} = Q_{3L}$	$u3 = u_{3R}$	$EI_3 \frac{du3^3}{dx^3} = -Q_{3R}$
$\frac{du3}{dx} = \theta_{3L}$	$EI_3 \frac{du3^2}{dx^2} = -M_{3L}$	$\frac{du3}{dx} = \theta_{3R}$	$EI_3 \frac{du3^2}{dx^2} = M_{3R}$
$\phi = \phi_{3L}$	$GK \frac{d\phi}{dx} = -T_{3L}$	$\phi = \phi_{3R}$	$GK \frac{d\phi}{dx} = T_{3R}$

The boundary conditions of sub element 1 and sub element 2 are applied back in the general solution expression equation (10). Then, the displacements (U) and forces (Q) matrices can be written in terms of coefficients $B_1, \dots, B_{14}$ for the two sub elements.

$$U = [M]B \tag{11}$$

$$Q = [N]B \tag{12}$$

for equation (11) and equation (12) the matrices of U, Q and B are as the followings:

$$U = [u_{1L}, \theta_{1L}, u_{2L}, \theta_{2L}, u_{3L}, \theta_{3L}, \phi_{3L}, u_{1R}, \theta_{1R}, u_{2R}, \theta_{2R}, u_{3R}, \theta_{3R}, \phi_{3R}]^T$$

$$Q = [Q_{1L}, M_{1L}, Q_{2L}, M_{2L}, Q_{3L}, M_{3L}, T_{3L}, Q_{1R}, M_{1R}, Q_{2R}, M_{2R}, Q_{3R}, M_{3R}, T_{3R}]^T$$

$$B = \left[B_1, B_2, B_3, B_4, B_5, B_6, B_7, B_8, B_9, B_{10}, B_{11,}, B_{12}, B_{13}, B_{14}\right]^T.$$

Matrices $[M]$ and $[N]$ is obtained for sub element 1 and for sub element 2 using the general solution expression in equation (10) and the boundary conditions of each sub elements. Then the DSM is obtained using equation (11) and equation (12) as the shown below,

$$Q = [N]A = [N][M]^{-1}U = [K]U$$

$$[K] = [N][M]^{-1} \tag{13}$$

Matrix $[K]$ elements is divided into either 3x3 or 4x4 sub matrices that results in 14x14 matrix. Each sub matrix is relating forces with displacements of the element. Where subscripts r and s are used for the rails and the slab respectively. While subscripts L and R are used for representing left and right hand-side of the element.

$$\begin{bmatrix} \bar{Q}_{rL} \\ \bar{Q}_{sL} \\ \bar{Q}_{rR} \\ \bar{Q}_{sR} \end{bmatrix} = \begin{bmatrix} K_{rL-rL} & K_{rL-sL} & K_{rL-rR} & K_{rL-sR} \\ K_{zL-rL} & K_{sL-sL} & K_{sL-rR} & K_{sL-sR} \\ K_{rR-rL} & K_{rR-sL} & K_{rR-rR} & K_{rR-sR} \\ K_{sR-rL} & K_{sR-sL} & K_{sR-rR} & K_{sR-sR} \end{bmatrix} \begin{bmatrix} \bar{u}_{rL} \\ \bar{u}_{sL} \\ \bar{u}_{rR} \\ \bar{u}_{sR} \end{bmatrix}$$

Two DSM for the two sub-elements $[K_{\mathrm{i}}]$ and $[K_{\mathrm{ii}}]$ are obtained. Subscripts i and ii refers to sub element 1 and sub element 2 respectively. After computing $[K_i]\ and\ [K_{ii}]$, matrix $[K_{element}]$ for the entire special FST element is obtained using joint boundary conditions between sub elements (Figure 25).

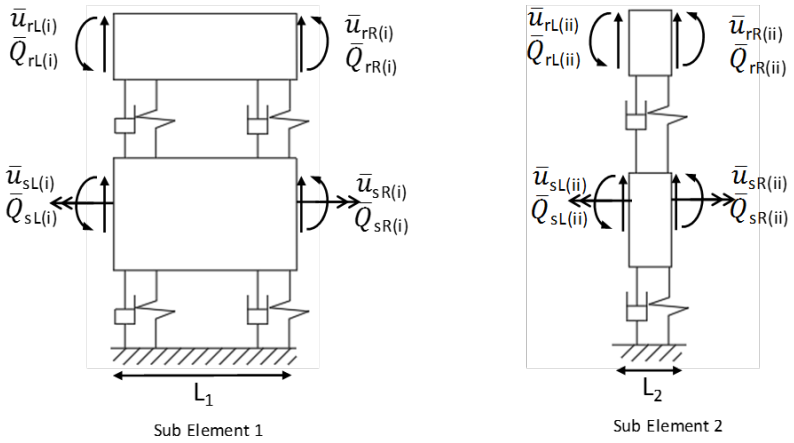

Figure 25: Boundary conditions of both sub elements (Side view).

Since the rails have a constant cross-section across sub-elements 1 and 2, the $[K]$ matrix for the two sub-elements is rearranged to obtain the $[K_{\text{element}}]$ matrix. As illustrated in equation (14), the rearranged $[K]$ matrix is relating slab segment's forces to the slab segment's displacements.

$$\begin{bmatrix} \bar{Q}_{sL} \\ \bar{Q}_{sR} \end{bmatrix} = \begin{bmatrix} K_{sL-sL} & K_{sL-sR} \\ K_{sR-sL} & K_{sR-sR} \end{bmatrix} \begin{bmatrix} \bar{u}_{sL} \\ \bar{u}_{sR} \end{bmatrix} \tag{14}$$

Then the slab boundary conditions (Figure 26) are used in the computations of DSM of two sub elements.

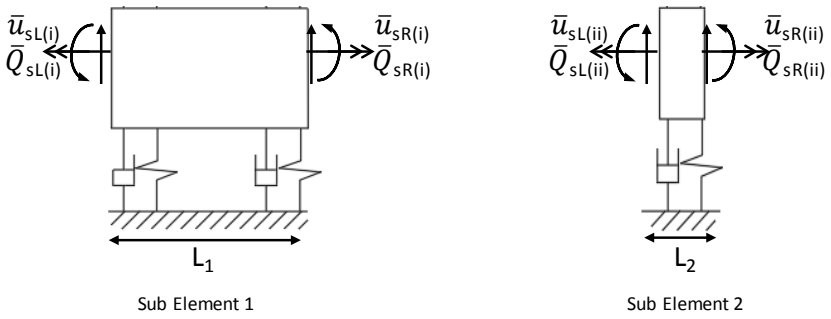

Figure 26: Boundary conditions of slab segments of the sub elements (Side view).

The equations for sub-elements 1 and 2 can be written as:

$$\begin{bmatrix} \bar{Q}_{sL(i)} \\ \bar{Q}_{sR(\mathrm{i})} \end{bmatrix} = [K_{\mathrm{i}}] \begin{bmatrix} \bar{u}_{sL(\mathrm{i})} \\ \bar{u}_{sR(\mathrm{i})} \end{bmatrix} \tag{15}$$

$$\begin{bmatrix} \bar{Q}_{sL(\mathrm{ii})} \\ \bar{Q}_{sR(ii)} \end{bmatrix} = [K_{\mathrm{ii}}] \begin{bmatrix} \bar{u}_{sL(ii)} \\ \bar{u}_{sR(ii)} \end{bmatrix} \tag{16}$$

the whole element matrix $[K_{element}]$ should relate the following slab's forces and displacements.

$$\begin{bmatrix} \bar{Q}_{sL(\mathrm{i})} \\ \bar{Q}_{sR(\mathrm{ii})} \end{bmatrix} = [K_{element}] \begin{bmatrix} \bar{u}_{sL(\mathrm{i})} \\ \bar{u}_{sR(\mathrm{ii})} \end{bmatrix} \tag{17}$$

Using the at joint conditions between the two sub elements (Equation 18), matrix $[K_{element}]$ is going to be formed from the DSM of the sub elements as the following:

At joint conditions

$$\bar{Q}_{sR(\mathrm{i})} = -\bar{Q}_{sL(\mathrm{ii})} \text{ and } \bar{u}_{sR(i)} = \bar{u}_{sL(\mathrm{ii})} \tag{18}$$

Writing required slab's forces for the special FST element in an equations form

$$\bar{Q}_{sL(\mathrm{i})} = K_{sL-sL(i)}\bar{u}_{sL(\mathrm{i})} + K_{sL-sR(i)}\bar{u}_{sR(\mathrm{i})} \tag{19}$$

$$\bar{Q}_{sR(\mathrm{ii})} = K_{sR-sL(ii)}\bar{u}_{sL(ii)} + K_{sR-sR(ii)}\bar{u}_{sR(ii)} \tag{20}$$

substituting the first at joint boundary condition in equations (18) ($\bar{Q}_{sR(\mathrm{i})} = -\bar{Q}_{sL(\mathrm{ii})}$) to the above equations

$$K_{sR-sL(i)}\bar{u}_{sL(i)} + K_{sR-sR(i)}\bar{u}_{sR(i)} = -K_{sL-sL(ii)}\bar{u}_{sL(ii)} - K_{sL-sR(ii)}\bar{u}_{sR(ii)} \tag{21}$$

using the other at joint boundary condition in equations (18) ($\bar{u}_{sR(i)} = \bar{u}_{sL(\mathrm{ii})}$) and substituting it in equation 21, equation 21 can be written as:

$$\bar{u}_{sR(i)} = \bar{u}_{sL(\mathrm{ii})} = -\left[K_{sR-sR(i)} + K_{sL-sL(ii)}\right]^{-1}K_{sL-sR(ii)}\bar{u}_{sR(\mathrm{ii})} - \left[K_{sR-sR(i)} + K_{sL-sL(ii)}\right]^{-1}K_{sR-sL(i)}\bar{u}_{sL(i)}$$

back substitution of the above equation in equation (19) and (20) gives:

$$\bar{Q}_{sL(i)} = K_{sL-sL(i)}\bar{u}_{sL(i)} + K_{sL-sR(i)}\left(-\left[K_{sR-sR(i)} + K_{sL-sL(ii)}\right]^{-1}K_{sL-sR(ii)}\bar{u}_{sR(ii)} - \left[K_{sR-sR(i)} + K_{sL-sL(ii)}\right]^{-1}K_{sR-sL(i)}\bar{u}_{sL(i)}\right)$$

$$\bar{Q}_{sR(ii)} = K_{sR-sR(ii)}\bar{u}_{sR(ii)} + K_{sR-sL(ii)}\left(-\left[K_{sR-sR(i)} + K_{sL-sL(ii)}\right]^{-1}K_{sL-sR(ii)}\bar{u}_{sR(ii)} - \left[K_{sR-sR(i)} + K_{sL-sL(ii)}\right]K_{sR-sL(i)}\bar{u}_{sL(i)}\right)$$

After using the at joint condition between the two sub elements, equation (19) and (20) turn out to represents the boundary conditions of the slab segment for the entire special FST element in terms of the slab's forces and displacements (Figure 27).

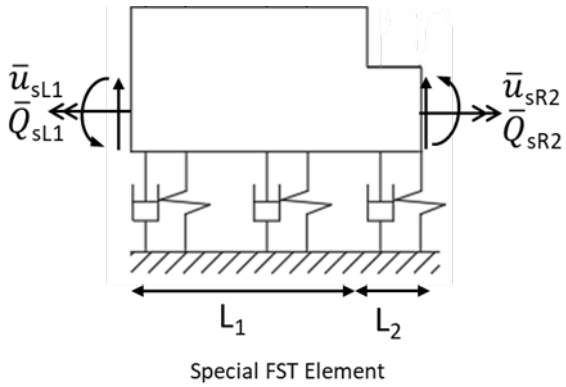

Figure 27: Boundary conditions of the slab segment of the special FST element (Side view).

Equation (19) and (20) is arranged to be written in a matrix form as the following:

$$\begin{bmatrix} \bar{Q}_{sL(i)} \\ \bar{Q}_{sR(ii)} \end{bmatrix} = \begin{bmatrix} K_{sL-sL(i)} - K_{sL-sR(i)} & -K_{sL-sR(i)} \\ \left[K_{sR-sR(i)} + K_{sL-sL(ii)}\right]^{-1} & \left[K_{sR-sR(i)} + K_{sL-sL(ii)}\right]^{-1} \\ K_{sR-sL(i)} & K_{sL-sR(ii)} \\ & \\ -K_{sR-sL(ii)} & K_{sR-sR(ii)} \\ \left[K_{sR-sR(i)} + K_{sL-sL(ii)}\right]^{-1} & \left[K_{sR-sR(i)} + K_{sL-sL(ii)}\right]^{-1} \\ K_{sR-sL(i)} & -K_{sR-sL(ii)}K_{sL-sR(ii)} \end{bmatrix} \begin{bmatrix} \bar{u}_{sL(i)} \\ \bar{u}_{sR(ii)} \end{bmatrix}$$

where the above DSM is the $[K_{element}]$.

To construct the full DSM of the special FST element including the rails, $[K_{element}]$ is substituted back in the DSM $[K]$ that relates forces and displacements of the rails and the slab for the entire special FST element.

$$\begin{bmatrix}\bar{Q}_{rL}\\ \bar{Q}_{sL}\\ \bar{Q}_{rR}\\ \bar{Q}_{sR}\end{bmatrix}=\begin{bmatrix} K_{rL-rL} & K_{rL-sL} & K_{rL-rR} & K_{rL-sR} \\ K_{zL-rL} & \begin{matrix} K_{sL-sL(i)}-K_{sL-sR(i)} \\ \left[K_{sR-sR(i)}+K_{sL-sL(ii)}\right]^{-1} \\ K_{sR-sL(i)} \end{matrix} & K_{sL-rR} & \begin{matrix} -K_{sL-sR(i)} \\ \left[K_{sR-sR(i)}+K_{sL-sL(ii)}\right]^{-1} \\ K_{sL-sR(ii)} \end{matrix} \\ K_{rR-rL} & K_{rR-sL} & K_{rR-rR} & K_{rR-sR} \\ K_{sR-rL} & \begin{matrix} -K_{sR-sL(ii)} \\ \left[K_{sR-sR(i)}+K_{sL-sL(ii)}\right]^{-1} \\ K_{sR-sL(i)} \end{matrix} & K_{sR-rR} & \begin{matrix} K_{sR-sR(ii)} \\ \left[K_{sR-sR(i)}+K_{sL-sL(ii)}\right]^{-1} \\ -K_{sR-sL(ii)}K_{sL-sR(ii)} \end{matrix} \end{bmatrix}\begin{bmatrix}\bar{u}_{rL}\\ \bar{u}_{sL}\\ \bar{u}_{rR}\\ \bar{u}_{sR}\end{bmatrix}$$

where the DSM of the entire special FST element that is relating the boundary forces with displacements of the element of the special FST is:

$$\begin{bmatrix} K_{rL-rL} & K_{rL-sL} & K_{rL-rR} & K_{rL-sR} \\ K_{zL-rL} & \begin{matrix} K_{sL-sL(i)}-K_{sL-sR(i)} \\ \left[K_{sR-sR(i)}+K_{sL-sL(ii)}\right]^{-1} \\ K_{sR-sL(i)} \end{matrix} & K_{sL-rR} & \begin{matrix} -K_{sL-sR(i)} \\ \left[K_{sR-sR(i)}+K_{sL-sL(ii)}\right]^{-1} \\ K_{sL-sR(ii)} \end{matrix} \\ K_{rR-rL} & K_{rR-sL} & K_{rR-rR} & K_{rR-sR} \\ K_{sR-rL} & \begin{matrix} -K_{sR-sL(ii)} \\ \left[K_{sR-sR(i)}+K_{sL-sL(ii)}\right]^{-1} \\ K_{sR-sL(i)} \end{matrix} & K_{sR-rR} & \begin{matrix} K_{sR-sR(ii)} \\ \left[K_{sR-sR(i)}+K_{sL-sL(ii)}\right]^{-1} \\ -K_{sR-sL(ii)}K_{sL-sR(ii)} \end{matrix} \end{bmatrix}$$

Since the DSM for the special FST element is obtained, the DSM for finite and infinite special FST tracks can be computed as illustrated in Section 3.3.3 and Section 3.3.4.

3.3.3 Fast Running Model of The Mockup

Qatar Rail mock up track is divided into number of elements based on slab cross section configurations. Each element has different slab cross section. There are four configurations of slab cross section distributed along the mockup (Figure 20). In this finite model, the special FST DSM obtained above is used to compute DSM for each element of the mockup following the same procedures illustrated in the above sections.

Since special FST DSM is used to compute the DSM of the mockup elements, the variation of the slab cross sections of the mockup track is taken into consideration. A global DSM of the mockup track is formed. The global stiffness matrix includes every DSM of each element of the mockup track.

The global DSM is arranged based on FE techniques. Each element has 3 nodes on the left and 3 nodes on the right. Every node in the track is given a number. The nodes represent the left and right end forces and displacements of each element. The global DSM of the track is relating forces and displacements of each element. Using the nodes number, the global DSM is arranged. Then, the response at any node on the track is obtained from the following relationship:

$$[\bar{u}_t] = [K_{Global}]^{-1}[F_t] \tag{22}$$

where [F] corresponds to the external forces applied on the nodes.

3.3.4 Fast Running Model of The Infinite Case

For the infinite case, the special FST is modelled using Periodic Structure theory which is utilized by implementing the Repeating-Unit Method to calculate DSM of the infinite track from the DSM of an element. The infinite track is divided into two semi-infinite tracks (Figure 28). The objective is to calculate DSM for a semi-infinite track. Then, DSM for the other semi-infinite track is calculated by using the boundary

conditions at the joint between the two semi-infinite tracks. Adding the DSMs of the two semi-infinite tracks together results in one DSM for the entire infinite track.

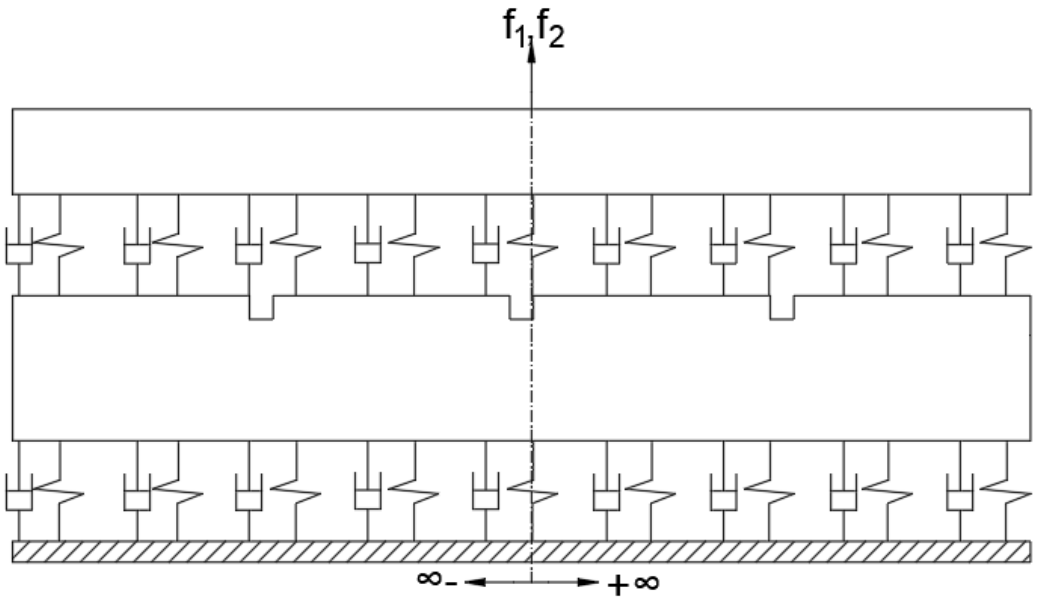

Figure 28: Division of the infinite track to two semi-infinite tracks.

Recalling the DSM of the specail FST element obtained in Section 3.3.2 to use it for computing DSM for the infinite track using Repeating Unit Method. The Repeating Unit Method uses the DSM of an element to genetrat $[T]$ matrix. $[T]$ matrix is called state matrix or transfer matrix. State matrix relates the state of displacements and forces at the left of j^{th+1} element to the state of displacements and forces at the left of j^{th} element.Displacements and forces state of the j^{th+1} and the j^{th} element are:

$$S^{j+1} = \left[\bar{u}_{rL}{}^{T} \quad \bar{u}_{sL}{}^{T} \quad \bar{Q}_{rL}{}^{T} \quad \bar{Q}_{rL}{}^{T}\right]^{T} \text{ and } S^{j} = \left[\bar{u}_{rL}{}^{T} \quad \bar{u}_{sL}{}^{T} \quad \bar{Q}_{rL}{}^{T} \quad \bar{Q}_{rL}{}^{T}\right]^{T} \quad (23)$$

The eqilibrium conditions between two succesive elements is used to write $[T]$ matrix. The displacments at the right hand side of j^{th} element is equal to that at left hand side of the j^{th+1} element. The forces at the right hand side of j^{th} element is equal and opposite to that at left hand side of the j^{th+1} element.

$$\begin{bmatrix} \overline{Q}_{rL} \\ \overline{Q}_{sL} \\ \overline{Q}_{rR} \\ \overline{Q}_{sR} \end{bmatrix}^{j^{th}} = \begin{bmatrix} \overline{Q}_{rL} \\ \overline{Q}_{sL} \\ 0 \\ 0 \end{bmatrix}^{j^{th}} + \begin{bmatrix} 0 \\ 0 \\ -\overline{Q}_{rL} \\ -\overline{Q}_{sL} \end{bmatrix}^{j^{th+1}} = [K] \begin{bmatrix} \overline{u}_{rL} \\ \overline{u}_{sL} \\ \overline{u}_{rR} \\ \overline{u}_{sR} \end{bmatrix}^{j^{th}} = [K] \left(\begin{bmatrix} \overline{u}_{rL} \\ \overline{u}_{sL} \\ 0 \\ 0 \end{bmatrix}^{j^{th}} + \begin{bmatrix} 0 \\ 0 \\ \overline{u}_{rL} \\ \overline{u}_{sL} \end{bmatrix}^{j^{th+1}} \right)$$

the above matrices can be simplified and condensed to

$$\begin{bmatrix} \overline{Q}_L{}^{j^{th}} \\ -\overline{Q}_L{}^{j^{th+1}} \end{bmatrix} = \begin{bmatrix} K_{L-L} & K_{L-R} \\ K_{R-L} & K_{R-R} \end{bmatrix} \begin{bmatrix} \overline{u}_L{}^{j^{th}} \\ \overline{u}_L{}^{j^{th+1}} \end{bmatrix} \tag{24}$$

also, matrices of (23) can be condensed to be written as:

$$S^{j+1} = \begin{bmatrix} \overline{u}_L \\ \overline{Q}_L \end{bmatrix} \text{ and } S^{j} = \begin{bmatrix} \overline{u}_L \\ \overline{Q}_L \end{bmatrix} \tag{25}$$

Equation (25) is used to make equation (24) relates the state of displacemnts and forces at the left hand-side of the j^{th+1} element to the state of displacemnts and forces at the left hand side of the j^{th} element, which will gives the transfer matrix

$$\begin{bmatrix} \bar{u}_L{}^{j^{th+1}} \\ -\bar{Q}_L{}^{j^{th}+1} \end{bmatrix} = \begin{bmatrix} -K_{L-R}{}^{-1}K_{L-L} & K_{L-R}{}^{-1} \\ K_{R-R}K_{L-R}{}^{-1}K_{L-L} - K_{L-R} & -K_{R-R}K_{L-R}{}^{-1} \end{bmatrix} \begin{bmatrix} \bar{u}_L \text{ג}^{j^{th}} \\ \bar{Q}_L{}^{j^{th}} \end{bmatrix} = [T] \begin{bmatrix} \bar{u}_L{}^{j^{th}} \\ \bar{Q}_L{}^{j^{th}} \end{bmatrix}$$

The solution of the above equation is based on Floquet's Theorem. The states propagate along the structure unchanged excepting the ampliude and phase. Then from j^{th} element to j^{th+1} element complex amplitiude modication factor (ג) is multiplied by the state of j^{th} element

$$S^{j+1} = [T]S^{j} \text{ and } S^{j+1} = \text{ג}S^{j} \tag{26}$$

equation (24) is presenting the statement of the Floquet's Theorem which gives

$$[T]S^{j} = \text{ג}S^{j} \tag{27}$$

This an eignvalue-eignvector problem in $[T]$ with eignvalues ג and eignvectors S^{j}. The state matrix $[T]$ is a 14x14 matrix, so there are 14 eignvalues corrosponding to 14 eignvectors.For absolute eignvalues less than 1, i.e $|\text{ג}| < 1$, the solution is decaying along the track as the distance from the excitation point increases. For absolute

eignvalue more than 1, i.e $|ג| > 1$, the solution is growing along the track as the distance from the excitation point increases. There are 7 eigenvalues representing each of the both solutions. Since the response of the excitation at free end must vanish as the distance from the excitation point goes to infinity, the 7 eigenvalues with $|ג| > 1$ and their corresponding eigenvectors are used to obtain the DSM for the semi-infinite track. The coefficients of each eigenvector are expressed as

$$C = [C_1 \quad C_2 \quad C_3 \quad C_4 \quad C_5 \quad C_6 \quad C_7]^T \tag{28}$$

The state at the free end of the left-hand side of the first element in the semi-infinite track is expressed as linear equation including 7 eigenvalues, 7 eigenvectors and their coefficients. Splitting the 7 eigenvectors between displacements and forces at the free end state results in

$$\bar{u}_{L@free\ end} = [\widehat{u_1} \quad \widehat{u_2} \quad \widehat{u_3} \quad \widehat{u_4} \quad \widehat{u_5} \quad \widehat{u_6} \quad \widehat{u_7}]^T C = [\hat{u}]C \tag{29}$$

$$\bar{Q}_{L@free\ end} = [\widehat{Q_1} \quad \widehat{Q_2} \quad \widehat{Q_3} \quad \widehat{Q_4} \quad \widehat{Q_5} \quad \widehat{Q_6} \quad \widehat{Q_7}]^T C = [\hat{Q}]C \tag{30}$$

where the hat indicates eigenvector quantity. Equation (29) and equation (28) are used to obtain 7x7 DSM matrix for the semi-infinite track. The DSM of the semi-infinite track relates the forces with the displacement at the free end

$$\bar{Q}_{L@free\ end} = [\hat{Q}][\hat{u}]^{-1}\bar{u}_{L@free\ end} = [K_{+\infty}]\bar{u}_{L@free\ end} \tag{31}$$

From DSM of one element of the track DSM for semi-infinite track is constructed. Using a FE technique for getting the DSM for the semi-infinite track, requires adding large number of elements together to obtain a converged response. Where, the repeating unit method involves only one simple computational step to obtain DSM for semi-infinite track.

The DSM for the other semi-infinite track $[K_{-\infty}]$ can be obtained by following the same procedures explained above. An alternative way to calculate it, is by using the symmetry condition of the track. The symmetry condition is only different at free end

of the other semi-infinite track. The sign of the obtained semi-infinite DSM $[K_{+\infty}]$ elements that relates the free end forces with rotations, free end moments with displacements and free end torque with displacements are changed. The DSM for the whole infinite track is obtained by adding the both DSMs of the two semi-infinite tracks together.

$$[K_{+\infty}] + [K_{-\infty}] = [K_{\infty}] \tag{32}$$

Then the response under the load can be obtained by using the below relation

$$\begin{bmatrix} \bar{u}_1 \\ \bar{u}_2 \\ \bar{u}_3 \end{bmatrix} = [K_{\infty}]^{-1} \begin{bmatrix} F1 \\ F2 \\ 0 \end{bmatrix} \tag{33}$$

where $\bar{u}_1$ and $\bar{u}_2$ are 2x1 submatrix representing the displacements and the rotations of the rails. $\bar{u}_3$ is 3x1 submatrix of displacement, rotation and angle of twist of the slab. External forces and moment applied on rails are F1 and F2. F1 and F2 are 2x1 sub matrix of $\begin{bmatrix} f_1 \\ 0 \end{bmatrix}$ and $\begin{bmatrix} f_2 \\ 0 \end{bmatrix}$ respectively. The external excitation f_1 and f_2 are set to equal to 1. There is no external moment on the rails, then it is equal to zero. There are no external forces, moment and torque on the slab, then it is equal to zero.

To find the state at any point on the track, the state at *n* units of the excitation point should be known first

$$S_n = C_1 \lambda_1 \bar{S}_1 + \cdots + C_7 \lambda_7 \bar{S}_7 \tag{34}$$

where, $\bar{S}$ and λ is the corresponding eigenvectors and eigenvalues of the state matrix $[T]$ for the decaying solutions. After finding the state at left hand side of the *n* unit from the excitation point, back substitution process can be followed to find the state at any point along the *n* unit. Obtained state matrix from equation (34) of the *n* unit is used to compute matrix $[N]$ and matrix $[M]$ to get the constant coefficients $B_1, \ldots, B_7$. By substituting the obtained constant coefficient in equation (11) and (12), the state is calculated at any point along the unit.

3.4 The Finite Element Model Formulation for The Mockup Track

In order to verify the mockup fast running model introduced in Section 3.3.4, a 3D FE model of the mockup FST was created using Abaqus 6.14 FE software [72]. The floating concrete slab was modeled using C3D8R solid elements (8-node linear brick with reduced integration), while the rails were modeled using B31 beam elements (2-node linear beam in space). The vertical stiffnesses of the rail fasteners and rubber pads were represented by linear spring elements (SPRINGA and SPRING1, respectively), while the viscous damping values were modeled using linear dashpot elements (DASHPOTA and DASHPOT1, respectively). A fine mesh with a nominal element size of 0.05 m was used, resulting in a total of 232736 elements and 263203 nodes.

The cross-sectional properties of the FST and rails along with the stiffness and damping values of the fasteners and pads are reported in Table 3. The values on Table 3 are per the drawings and the specifications provided by the manufacturer.

A frequency extraction analysis was carried out in Abaqus using Lanczos eigenvalue solver and the high-performance SIM architecture to identify the natural frequencies and mode shapes up to 80 Hz.

Table 3: Initial Model Parameters.

ID	Quantity	Description	Value
1	$L_{s,1}$	Length of segment 1 of the slab (m)	3.80
2	$L_{s,2}$	Length of segment 2 of the slab (m)	0.30
3	$L_{s,3}$	Length of segment 3 of the slab (m)	0.10
4	$L_{s,4}$	Length of segment 4 of the slab (m)	0.05
5	L	Total slab length (m)	16.7
6	$m_{r,1}, m_{r,2}$	Rail mass (kg/m)	76.284
7	$m_{s,1}$	Mass of segment 1 of the slab (kg/m)	4261.68
8	$m_{s,2}$	Mass of segment 2 of the slab (kg/m)	3452.64
9	$m_{s,3}$	Mass of segment 3 of the slab (kg/m)	2508.00
10	$m_{s,4}$	Mass of segment 4 of the slab (kg/m)	3317.04
11	$EI_{r,1}, EI_{r,2}$	Bending stiffness of the rail ($\mathrm{Pa \cdot m^4}$)	7.46×10^{6}
12	$EI_{s,1}$	Bending stiffness of segment 1 of the slab ($\mathrm{Pa \cdot m^4}$)	1.61×10^{9}
13	$EI_{s,2}$	Bending stiffness of segment 2 of the slab ($\mathrm{Pa \cdot m^4}$)	1.33×10^{9}
14	$EI_{s,3}$	Bending stiffness of segment 3 of the slab ($\mathrm{Pa \cdot m^4}$)	3.98×10^{8}
15	$EI_{s,4}$	Bending stiffness of segment 4 of the slab ($\mathrm{Pa \cdot m^4}$)	8.47×10^{8}
16	$GK_{s,1}$	Torsional rigidity of segment 1 of the slab ($\mathrm{Pa \cdot m^4}$)	1.74×10^{9}
17	$GK_{s,2}$	Torsional rigidity of segment 2 of the slab ($\mathrm{Pa \cdot m^4}$)	1.38×10^{9}
18	$GK_{s,3}$	Torsional rigidity of segment 3 of the slab ($\mathrm{Pa \cdot m^4}$)	5.32×10^{8}
19	$GK_{s,4}$	Torsional rigidity of segment 4 of the slab ($\mathrm{Pa \cdot m^4}$)	8.17×10^{8}
20	J_s	Mass polar moment of inertia of the slab ($\mathrm{kg \cdot m^2/m}$)	2400
21	k_1, k_2	Stiffness of rail fasteners ($\mathrm{N/m/m}$)	2.03×10^{7}
22	k_3, k_4	Stiffness of slab bearings ($\mathrm{N/m/m}$)	2.52×10^{6}
23	c_1, c_2	Damping of rail fasteners ($\mathrm{N \cdot s/m/m}$)	1.49×10^{4}
24	c_3, c_4	Damping of slab bearings ($\mathrm{N \cdot s/m/m}$)	3.74×10^{4}
25	b	Distance between rails (m)	1.50

CHAPTER 4: MODEL VERIFICATION, VALIDATION AND UPDATING PROCESS

4.1 Introduction

In this chapter the fast running model created in the previous chapter is verified, validated and updated.

The verification section in this chapter includes the comparison of the transfer functions obtained from the fast running model of the mockup to those from the FE model. The transfer function of eight points due to a single harmonic concentrated load applied at the center of one of the rails are used in this comparison, where six points are located on the rails and two points are on the slab.

For the validation process in this chapter, an experimental test is used to validate the fast running model. The experimental test is performed to explore the actual transfer function of the mock up track. Similar to the verification process, the response of eight points on the track due to an impulse excitation at the center of one of the rails are obtained. The obtained results from the experimental test are compared to those from the fast running model.

Finally, this chapter contains a model updating process as an attempt to improve the agreement between the predicted and observed responses. A hybrid optimization process was carried out to automatically refine the parameters of the fast running model. This process merges a Genetic Algorithm (GA) as a global optimization tool with a local search strategy.

4.2 Model Verification

A Matlab [74] function was written to carry out the computations discussed in Section 3.3.4 for the fast running model of the mock up track. The input parameters were introduced per Table 3. The acceleration response under the aforementioned loading scenario was computed at 8 points shown in Figure 29 (6 points on the rails and 2 points on the slab) and then compared to the results obtained using the Abaqus FE model.

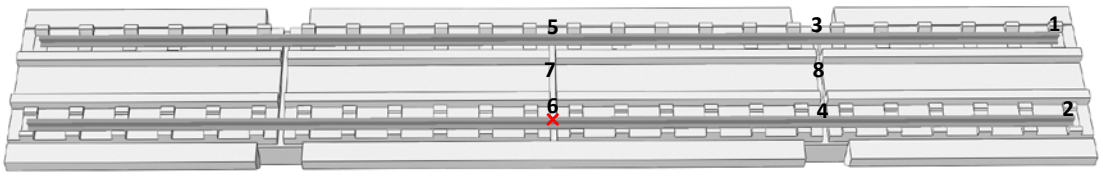

Figure 29: The locations of the 8 points at which the response was computed. Points 1 to 6 are on the rails. Points 7 and 8 are on the slab. The red cross represents the location of the concentrated harmonic load (Point 6).

For the Abaqus FE model., the natural frequencies and mode shapes up to 80 Hz were obtained using frequency extraction analysis as mentioned in Section 3.4. The first natural frequency was 5.26 Hz corresponding to the resonance of the slab on its bearings, which can be estimated as:

$$f = \frac{1}{2\pi}\sqrt{\frac{K_{\text{bearings}}}{M_{\text{slab}}}} = \frac{1}{2\pi}\sqrt{\frac{L(k_3 + k_4)}{4M_1L_1 + 4M_2L_2 + 2M_3L_3 + M_4L_4}} \tag{35}$$

The bending and torsional modes of the free-free slab model are presented in Figure 30. The frequency extraction process was followed by a mode-based steady - state dynamic analysis in the frequency domain to compute the dynamic response due to a single harmonic concentrated load applied at the center of one of the rails.

The comparison provided in Figure 31 shows good agreement between the transfer functions computed using the fast running model and those estimated using the 3D FE model. Discrepancies can be noticed especially around the frequency of the 3rd bending mode (41 Hz for the fast running model compared to 38 Hz for the 3D FE model). This can be attributed to the limitations of Euler-Bernoulli beam model which was used to formulate the numerical model. Another possible reason for this discrepancy is the fact that the point springs were used to represent the rail fasteners and slab bearings in Abaqus, while continuous layers of springs were assumed in the numerical model. Regardless, it can be stated that the fast running model and the FE model transfer functions are in very good correlation.

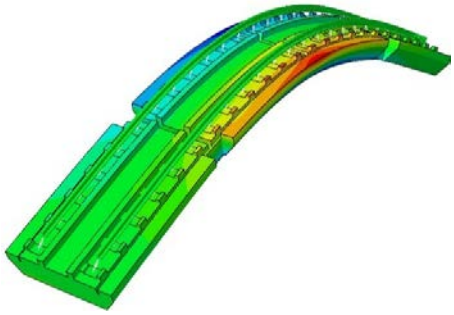

(1st bending mode: 9.14 Hz)

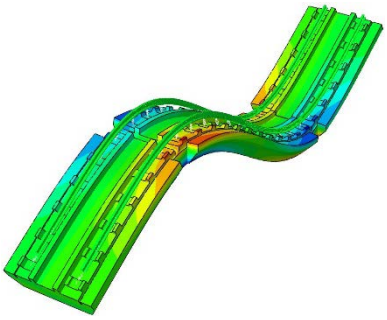

(2nd bending mode: 20.47 Hz)

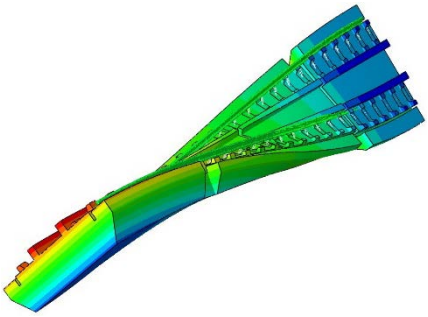

(1st torsional mode: 25.36 Hz)

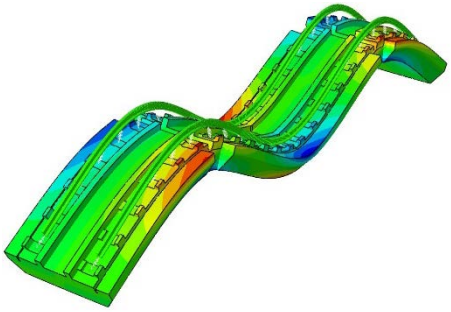

(3rd bending mode: 38.08 Hz)

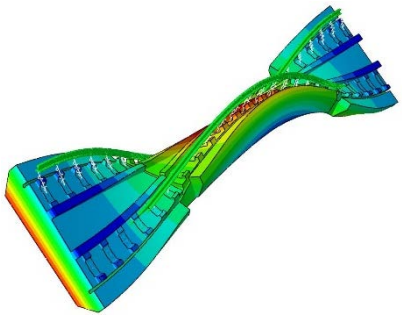

(2nd torsional mode: 48.53 Hz)

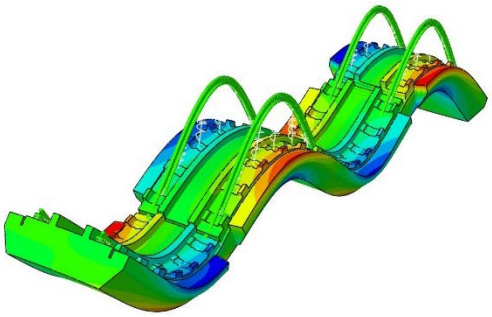

(4th bending mode: 66.65 Hz)

Figure 30: The first six bending and torsional modes of the mockup computed using Abaqus

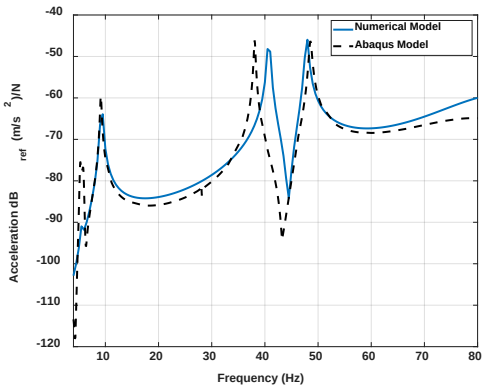

(Point 1)

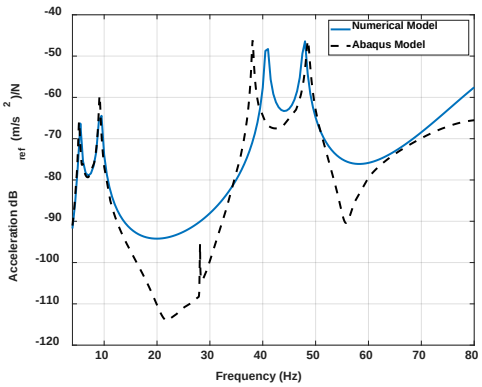

(Point 2)

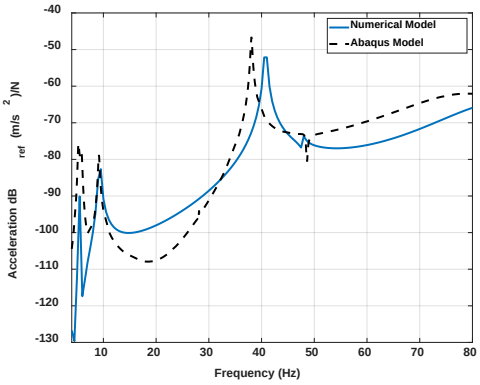

(Point 3)

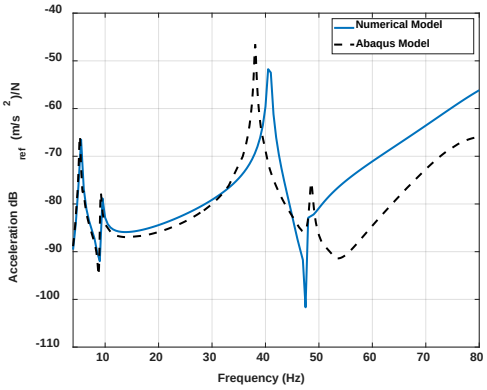

(Point 4)

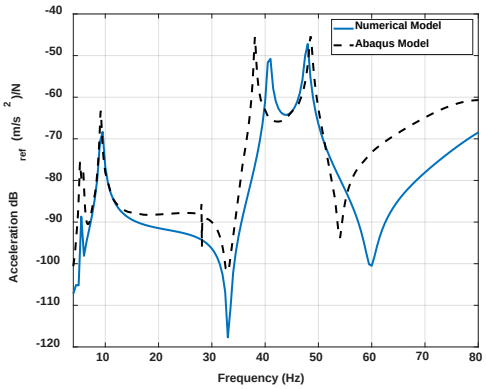

(Point 5)

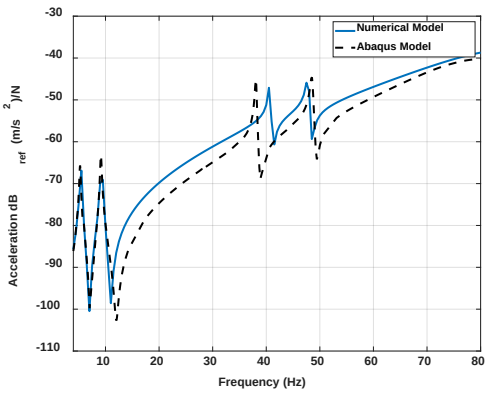

(Point 6)

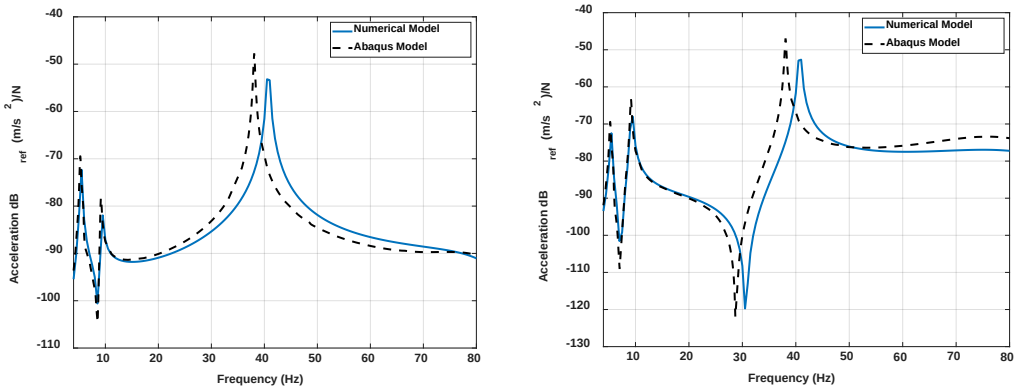

(Point 7) (Point 8)

Figure 31: Transfer Function comparison between the results obtained using the fast running model and the ones computed for the Abaqus 3D FE model

4.3 Experimental Test and Model Validation

After the fast running model study and the FE model verification, an impact test was carried out to identify the vibration response of the mockup FST experimentally. A modal sledge hammer (B&K model 8210, Figure 32) was used to apply an impulse excitation at the center of one of the rails (Point 6 in Figure 29). Since the frequency range of interest in this work is 3-80 Hz, the soft tip of the hammer was used to avoid exciting higher frequencies. B&K accelerometers (model 8344) were used to measure the vibration response under the impulse force at the 8 points shown in Figure 29. As depicted in Figure 33a, PCB model 080A121 magnetic mounts were used to attach the accelerometers to the rails (Points 1 to 6). To attach the accelerometers to the concrete slab (Points 7 & 8), 1.5×1.5 cm steel plates were glued to the slab, and the magnetic mounts were inserted on top of them as shown in Figure 33b.

Figure 32: B&K model 8210 impact hammer

(a) (b)

Figure 33: B&K model 8344 accelerometers attached to: (a) the rail, (b) the slab.

A 16-channel data acquisition device (model DT9857E-16) was used to collect the force and acceleration data. The modal analysis software ME'ScopeVES [75] was used to handle the data acquisition and processing operations. The test consisted of 10 hammer impacts, each applied within a window of 8 s. The sampling frequency was taken as 2048 Hz, resulting is a frequency resolution of 0.125 Hz. Each transfer function

was determined by averaging the 10 records to minimize random noise. For all measurement points, coherence values close to 1.0 were observed across the frequency range of interest. This indicated a good correlation between the impulse excitation and the acceleration signals [76].

Figure 34 compares the transfer function under the load (point 6) that is obtained experimentally to that estimated using the fast running model of the mockup according to the initial parameters of Table 3. The comparison shows a mismatch between the experimental and numerical results. This indicates that the initial model parameters should be fine-tuned to improve the agreement between the predicted and observed response.

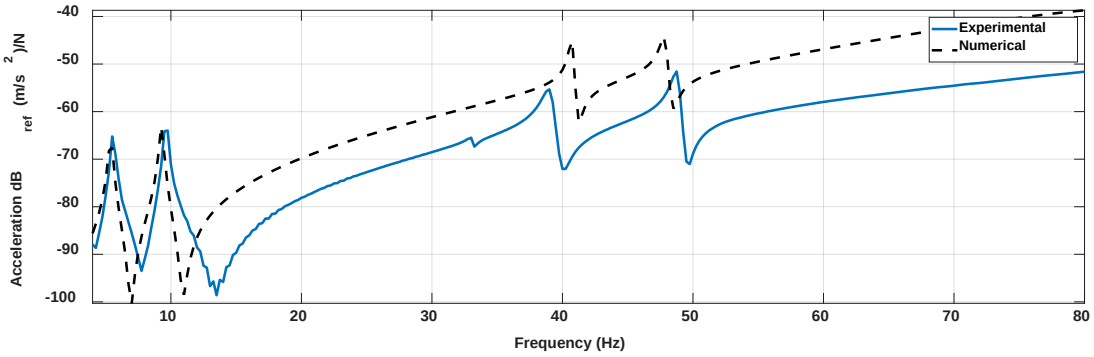

Figure 34: Transfer function comparison between the experimental and numerical response at Point 6.

4.4 Model Updating Process

Model updating process utilize a hybrid optimization process to automatically enhance the initial parameters of the fast running model. The hybrid optimization process combines a GA as a global optimization tool with a local search strategy. The aim of this process is to improve the matching between the predicted and observed response by fine-tuning the parameters of the fast running model.

A Matlab routine was written to act as the objective function of this optimization problem. The inputs to this routine are those related to the bending and torsional stiffness of the rails and the four slab cross-sections (parameters 11 to 20 in Table 3) along with the stiffness and damping of the rail fasteners and slab bearings (parameters 21 to 24 in Table 3). The first output of the routine, $\mathrm{NMSE}_{\mathrm{real}}$, is the normalized mean square error between the real part of the experimental response at Point 6 and the real part of the response computed numerically at this point. Similarly, the second output, $\mathrm{NMSE}_{\mathrm{imag}}$, represents the goodness-of-fit between the imaginary parts of the experimental and numerical responses at the same point.

Matlab Optimization Toolbox [74] was then used to carry out the global optimization process according to a multi-objective GA [77]. Appropriate lower and upper bounds were imposed on the 14 optimization variables to limit the solution space and ensure reasonable results. The population size was taken as 200 individuals. The selection process was handled by a tournament selection function. The cross-over fraction was set as 0.8, which means that 80% of each generation was produced by cross-over, while the remaining individuals were obtained by mutation. The global optimization process converged after 43 iterations. Figure 35 presents the comparison of the transfer functions for the experimental real and imaginary parts of the response at Point 6 to those obtained numerically using the updated parameters. It is observed

that there is an excellent match between the numerical and experimental transfer functions indicating that the optimization process was successful.

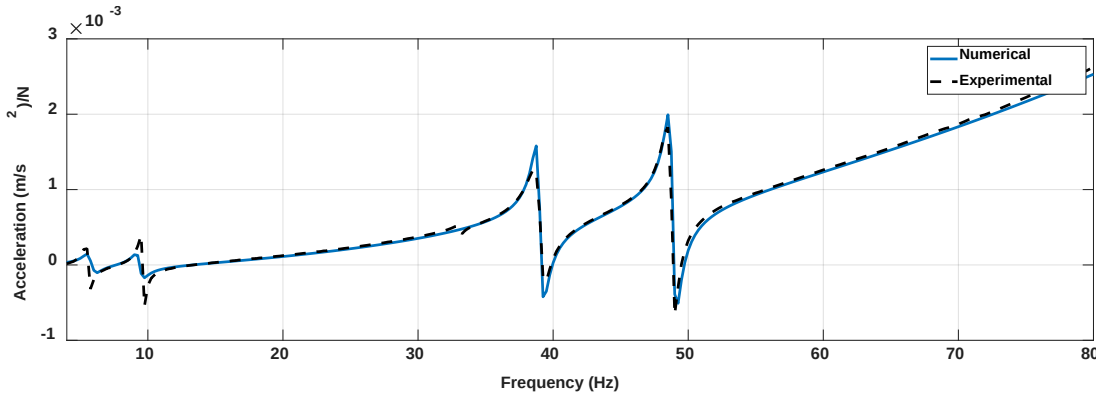

(a)

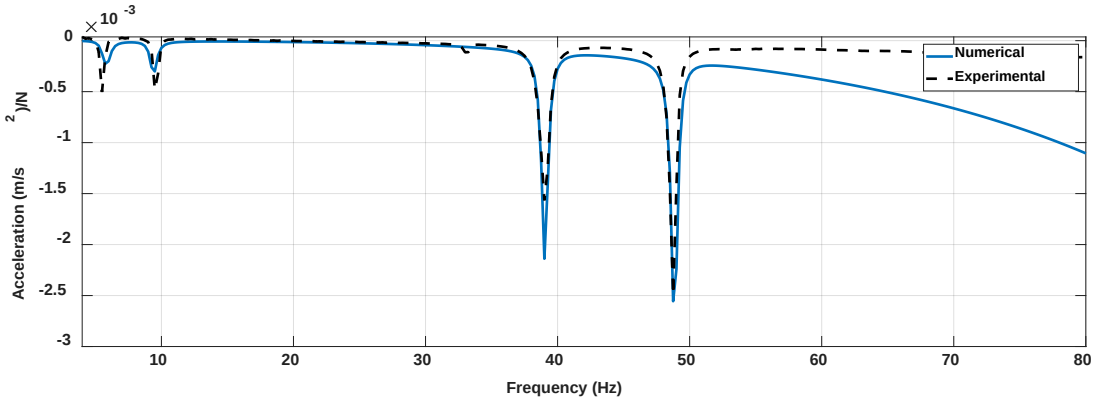

(b)

Figure 35: Comparison between the experimental and numerical response at Point 6 after running the global optimization process. (a) Real part. (b) Imaginary part.

Using Sequential Quadratic Programming (SQP) algorithm, a constrained local optimization process was conducted to further refine the model parameters. This algorithm is implemented in Matlab under the function “fmincon”. The solution obtained using GA was used as a starting point for the local search process. The objective function was taken as the NMSE between the magnitude of the experimental response at Point 6 and that computed numerically at the same point. The optimization process converged to the solution provided in Table 4.

Table 4: Final Results of the Model Updating Process.

ID	Quantity	Description	Value
11	$EI_{r,1}, EI_{r,2}$	Bending stiffness of the rail ($\mathrm{Pa \cdot m^4}$)	8.8285×10^{6}
12	$EI_{s,1}$	Bending stiffness of segment 1 of the slab ($\mathrm{Pa \cdot m^4}$)	1.5321×10^{9}
13	$EI_{s,2}$	Bending stiffness of segment 2 of the slab ($\mathrm{Pa \cdot m^4}$)	9.45×10^{8}
14	$EI_{s,3}$	Bending stiffness of segment 3 of the slab ($\mathrm{Pa \cdot m^4}$)	3.3×10^{8}
15	$EI_{s,4}$	Bending stiffness of segment 4 of the slab ($\mathrm{Pa \cdot m^4}$)	1.0283×10^{9}
16	$GK_{s,1}$	Torsional rigidity of segment 1 of the slab ($\mathrm{Pa \cdot m^4}$)	1.8329×10^{9}
17	$GK_{s,2}$	Torsional rigidity of segment 2 of the slab ($\mathrm{Pa \cdot m^4}$)	1.4574×10^{9}
18	$GK_{s,3}$	Torsional rigidity of segment 3 of the slab ($\mathrm{Pa \cdot m^4}$)	1.4061×10^{9}
19	$GK_{s,4}$	Torsional rigidity of segment 4 of the slab ($\mathrm{Pa \cdot m^4}$)	1.2354×10^{9}
20	J_s	Mass polar moment of inertia of the slab ($\mathrm{kg \cdot m^2/m}$)	2.5781×10^{3}
21	k_1, k_2	Stiffness of rail fasteners ($\mathrm{N/m/m}$)	6.0451×10^{7}
22	k_3, k_4	Stiffness of slab bearings ($\mathrm{N/m/m}$)	3.0180×10^{6}
23	c_1, c_2	Damping of rail fasteners ($\mathrm{N \cdot s/m/m}$)	5.0527×10^{4}
24	c_3, c_4	Damping of slab bearings ($\mathrm{N \cdot s/m/m}$)	7.7541×10^{3}

Figure 36 compares between the experimental transfer functions and those computed numerically using the parameters obtained by the model updating process. While the fast running was fine-tuned based exclusively on the response at Point 6, Figure 15 indicates that the model was able to accurately predict the response at the other 7 points. This clearly shows that the fast running model developed in this work is successful and, given the right parameters, it can be confidently used for estimating the vibration response of the special FST type represented by the mockup track.

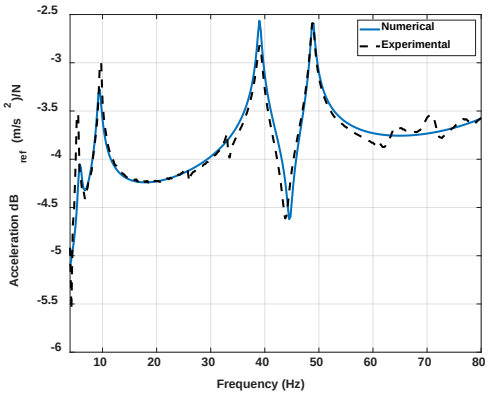

(Point 1)

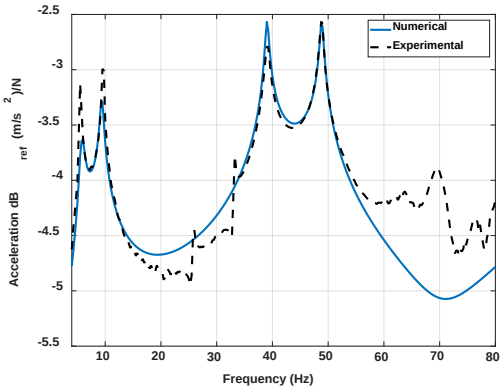

(Point 2)

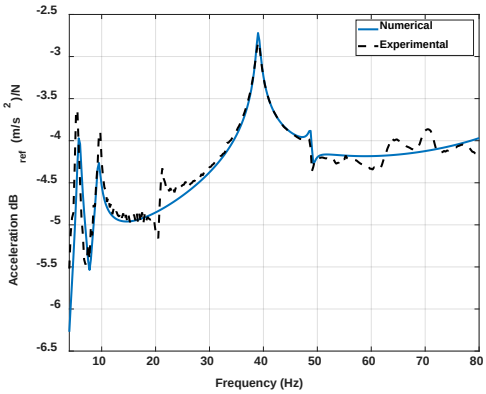

(Point 3)

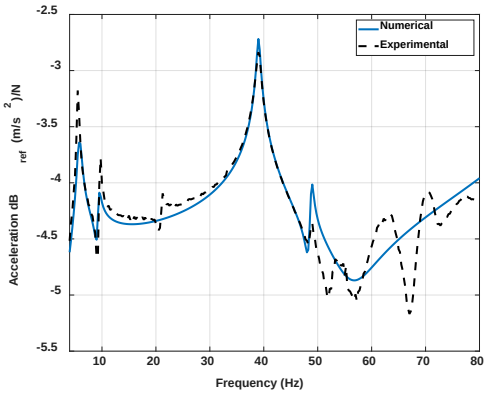

(Point 4)

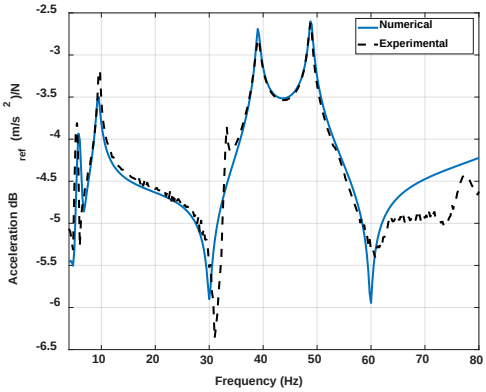

(Point 5)

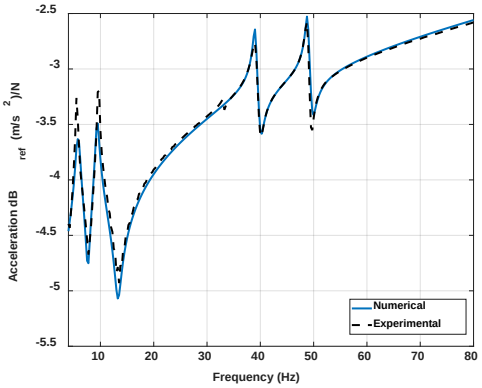

(Point 6)

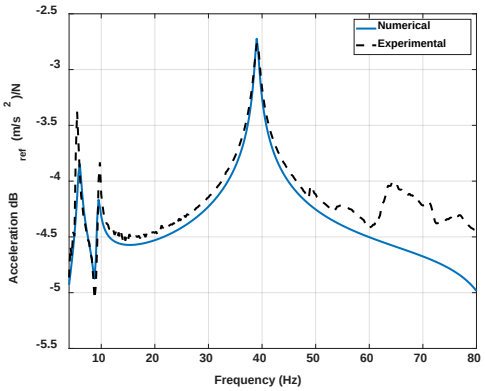

(Point 7)

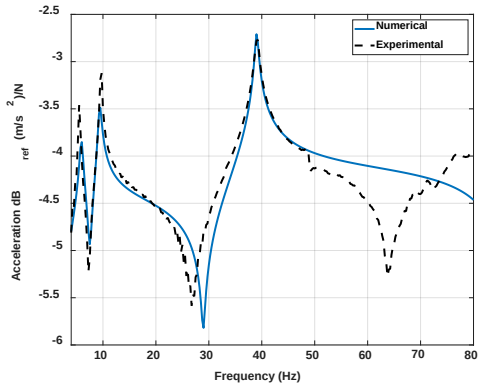

(Point 8)

Figure 36: Transfer function comparison between the experimental and numerical response after model updating for the 8 points.

CHAPTER 5:PARAMETRIC STUDY

5.1 Introduction

In this chapter, a parametric study is conducted based on the fine-tuned parameters obtained by the model updating procedures in the previous chapter in Section 4.4. The purpose of the parametric study is to characterize the effect of varying the depth of the grooves on the response of the infinite special FST design.

The study is including both bending and torsion loading scenarios. The infinite track model described previously in Section 3.3.4 was adopted for this study. A reduction factor representing the change of the slab depth with respect to the main cross-section is implemented in the parametric study.

The bending and torsional response of the rails and slab is going to be investigated for different values of the reduction factor. Varying the reduction factor value is going to produce different slab segment's parameters corresponding to the slab cross section at the grooves.

5.2 Results of The Parametric Study

The floating slab was modeled as a beam with two cross-sections only as illustrated in Figure 21b. The length of the main slab cross-section is L_1 while the width of the groove is L_2. For simplicity, an equivalent rectangular cross-section with dimensions of $B_S \times T_S$ was assumed for the main cross-section. Also, another rectangular cross-section with dimensions of $B_S \times \alpha T_S$ was taken at the groove, where B_S and T_S are the width and the thickness of the main cross section respectively. α is the reduction factor representing the change of the slab depth with respect to the main cross-section. The factor starts from 1 for a purely continuous beam and approaches to zero as the groove depth increases.

The length of the main cross-section L_1 was taken as 4.1 m, while the width of the groove was selected as $L_2 = 0.1$ m. The bending stiffness of the rails along with the damping and stiffness properties of the fasteners and slab bearings were taken directly from Table 4. When studying the effect of α under pure bending, the width B_s, depth T_s, modulus of elasticity E_s, and density ρ_s of the equivalent cross-section were chosen such that its mass m_s and bending stiffness EI_s are equal to $m_{s,1}$ and $EI_{s,1}$ in Table 4, respectively. Likewise, for analyzing the pure torsional response, B_s, T_s, ρ_s, along with the slab's shear modulus G_s were selected such that J_s and GK_s of the rectangular cross-section are analogous to their counterparts in the main cross-section of the mockup (J_s and $GK_{s,1}$ in Table 4). The properties of the equivalent cross-section for bending and torsion are summarized in Table 5.

Table 5: Geometry and Material Properties of the Equivalent Rectangular Sections for Pure Bending and Pure Torsion Cases.

Bending	Torsion
$B_s = 2.854$ m	$B_s = 2.596$ m
$T_s = 0.634$ m	$T_s = 0.694$ m
$E_S = 25.27 \times 10^9$ Pa	$G_S = 7.603 \times 10^9$Pa
$\rho_s = 2354$ kg/m^3	$\rho_s = 2375$ kg/m^3

Figure 36 shows the displacement transfer function of the rails and slab in pure bending calculated at the point of load application for different levels of α. For the continuous slab (i.e. $\alpha = 1$), a single peak can be noticed around 6 Hz corresponding to the resonant frequency of the slab on its bearings, which can be estimated as $f = \frac{1}{2\pi}\sqrt{\frac{k_3+k_4}{m_s}}$. For reduction factors larger than $\alpha = 0.6$, it appears that the grooves have a negligible effect on the response. However, at $\alpha = 0.5$, a small peak can be observed around 46 Hz. The frequency of this peak decreases with α to 33 Hz at $\alpha = 0.3$ down to 8 Hz for the nearly discontinuous case ($\alpha = 0.01$). The peak's frequency at $\alpha = 0.01$ is close to the first bending natural frequency of a free-free rail supported over intermediate supports at L_1 intervals, which can be estimated as [78]:

$$f = \frac{1.539^2}{2\pi L_1^2}\sqrt{\frac{EI_{r,1}}{m_{r,1}}} \tag{36}$$

Another peak becomes visible at 190 Hz starting from $\alpha = 0.5$. The peak's frequency decreases with α until reaching 127 Hz at $\alpha = 0.01$. This frequency corresponds to the first bending natural frequency of a free-free slab segment having a length of L_1, which can be computed as [78]:

$$f = \frac{4.73^2}{2\pi L_1^2}\sqrt{\frac{EI_s}{m_s}} \tag{37}$$

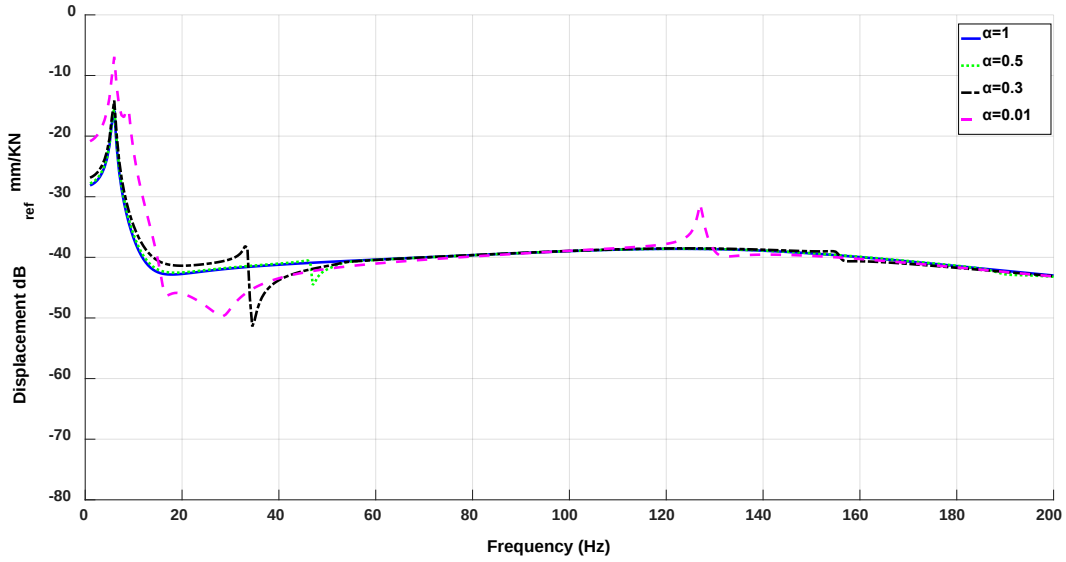

(a)

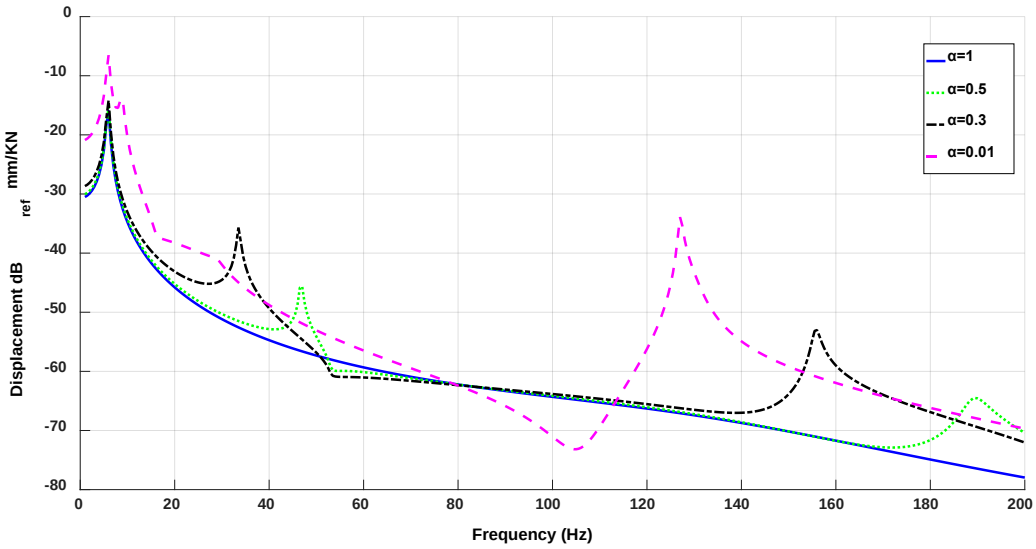

(b)

Figure 37: The displacement transfer function of (a) the rails and (b) the slab in pure bending calculated at the point of load application for different levels of α.

The results of varying α on the displacement response of the rails and slab under pure torsion are provided in Figure 38. Note that the displacement response of the slab was computed at its edge by multiplying the twist angle by $b/2$, where $b = 1.5$ m is the distance between rails. Similar to the bending case, a single peak can be noticed around 6 Hz corresponding to the resonance frequency of the slab on its bearings. Starting around $\alpha = 0.5$, a peak appears at 99 Hz. As α decrease, the amplitude of this peak increases without a noticeable change in its frequency. This frequency is associated with the first torsional natural frequency of a free-free slab segment having a length of L_1, given as [78]:

$$f = \frac{1}{2L_1}\sqrt{\frac{GK_s}{I_{p,s}\rho_s}} \tag{13}$$

where $I_{p,s}$ is the polar area moment of inertia of the slab's main cross-section.

Finally, Figures 39 and 40 show the displacement response of the rails and slab at a distance of 100 m from the point of load application in pure bending and torsion, respectively. At $\alpha = 0.5$ and $\alpha = 0.3$, the vibration response in both bending and torsion exhibits a large number of peaks. This behavior can be attributed to the complex interference between the slab units along the track. For the nearly discontinues case ($\alpha = 0.01$), it is observed that the vibration response over most of the frequency range is negligible as it is dominated by evanescent waves and leaky waves which decay dramatically with distance.

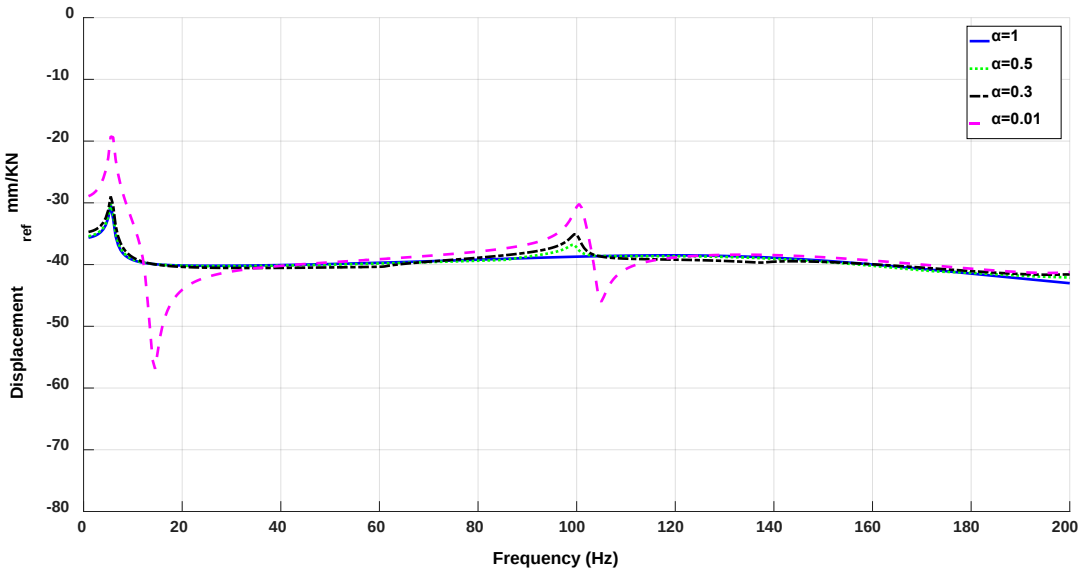

(a)

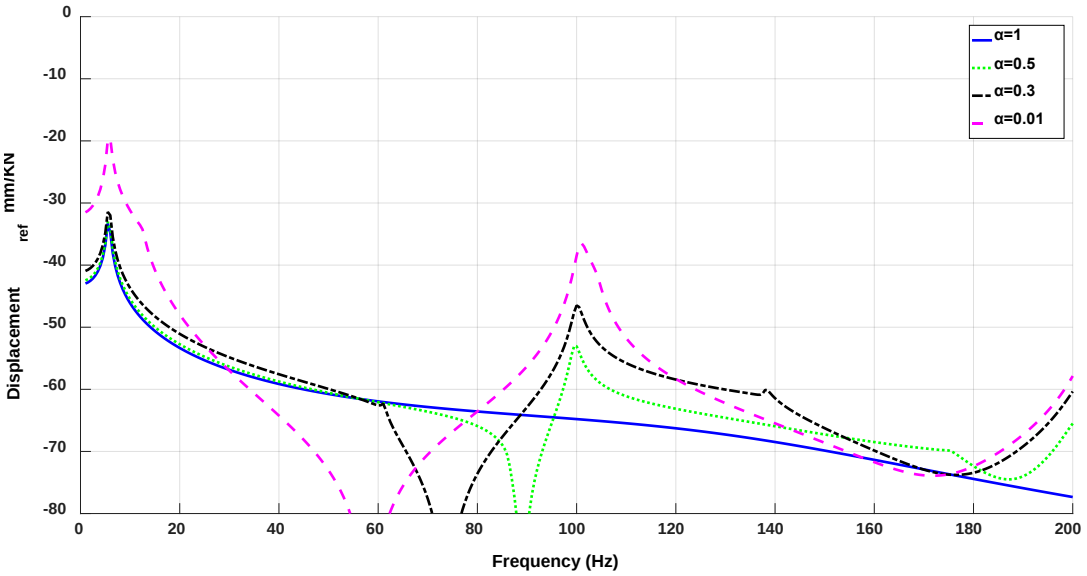

(b)

Figure 38: The displacement transfer function of (a) the rails and (b) the slab in pure torsion calculated at the point of load application for different levels of α.

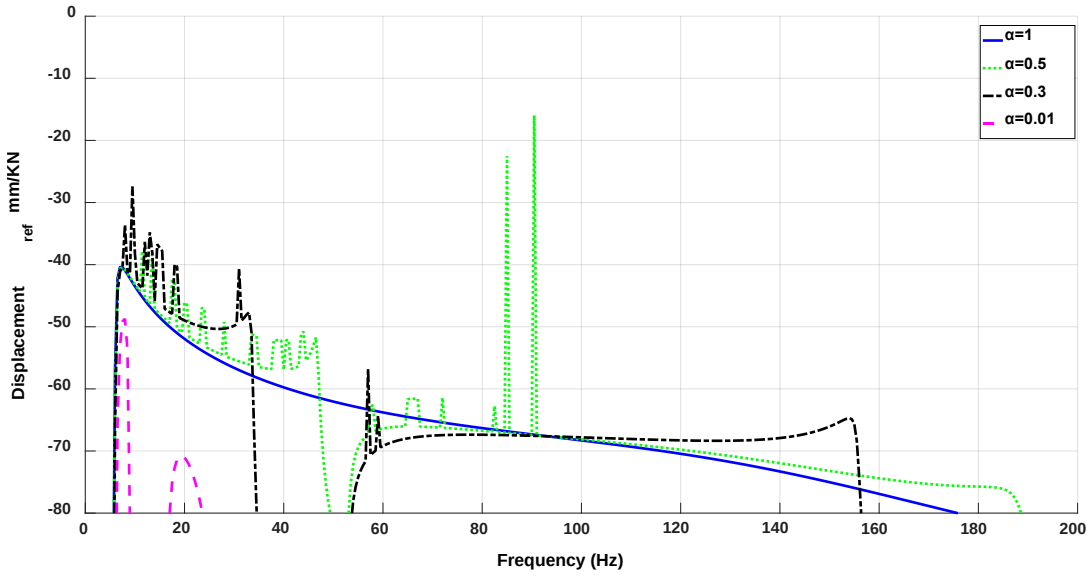

(a)

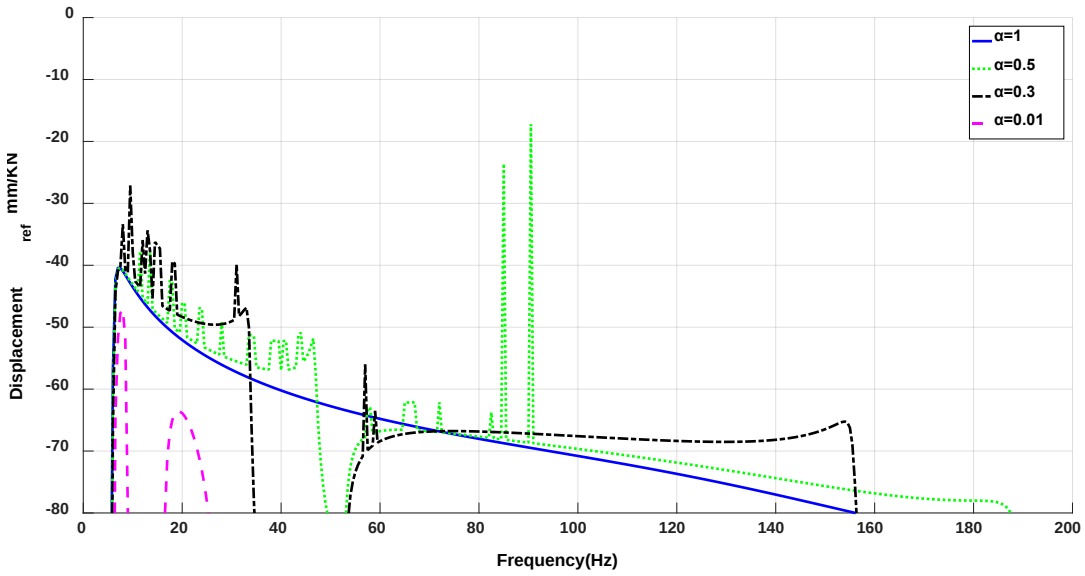

(b)

Figure 39: The displacement transfer function of (a) the rails and (b) the slab in pure bending calculated at a distance of 100 m from the point of load application for different levels of α.

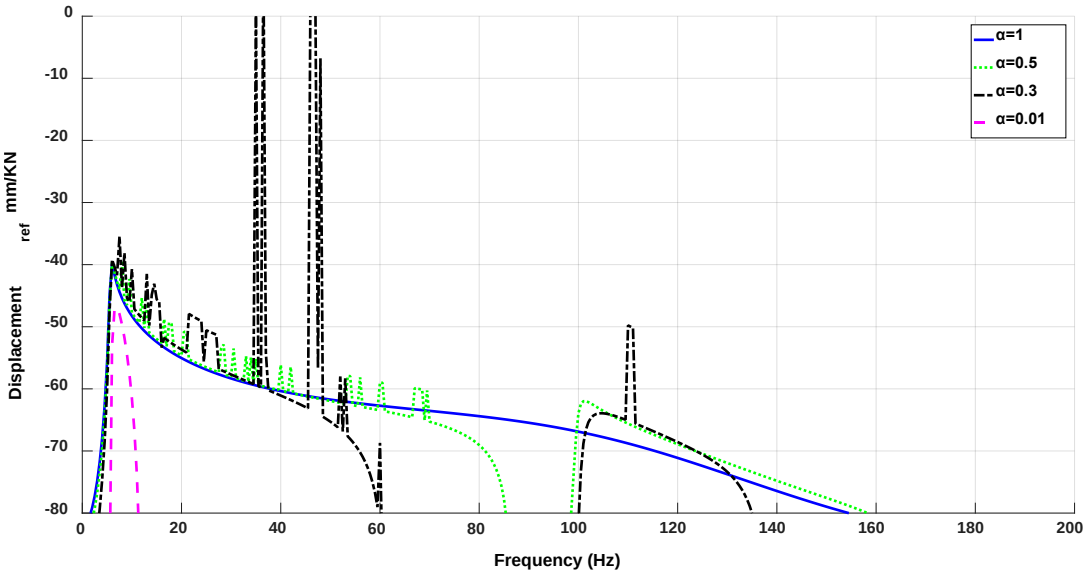

(a)

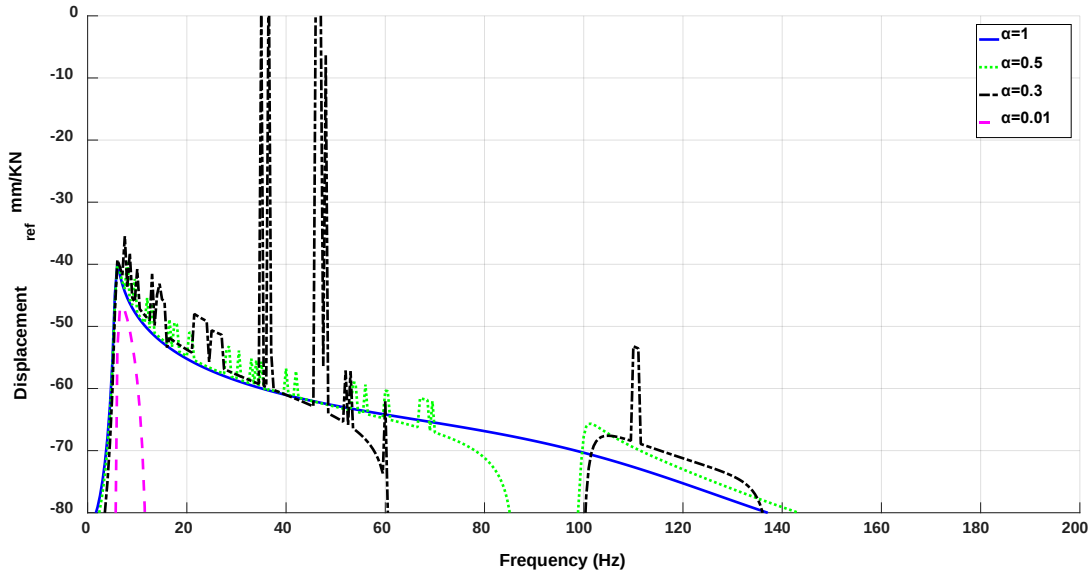

(b)

Figure 40: The displacement transfer function of (a) the rails and (b) the slab in pure torsion calculated at a distance of 100 m from the point of load application for different levels of α.

CHAPTER 6:CONCLUSIONS

This thesis presented a model for investigating the dynamic behavior of a special FST design. The floating concrete slab of this special track is composed of a repeating slab unit consisting of two segments with different cross sections, resulting in periodic grooves along the track. A fast running model based on Dynamic Stiffness method along with a detailed FE model were developed for a full-scale mockup structure. An experimental vibration test was then carried out to identify the actual vibration response of the structure. A hybrid model updating process that combines genetic algorithms with a local search method was conducted to systematically adjust the initial parameters of the fast running model. The updated model was then implemented in a parametric study to investigate the effect of changing the thickness of the grooves on the dynamic behavior of infinite special FST for both bending and torsion.

The results of the parametric study showed that the conventional continuous FST models can be used to accurately predict the vibration response of the special FST as long as the slab thickness at the groove is larger than 50% of the original beam thickness. Below that, it is necessary to use the proposed fast running model since the effect of the local bending and torsional modes of the slab units becomes significant.

REFRENCES

1. British Standards, I., *Guide to measurement and evaluation of human exposure to whole-body mechanical vibration and repeated shock*. 1999: British Standards Institution.
2. Duarte, M.L.M. and M.d.B. Pereira, *Vision influence on whole-body human vibration comfort levels.* Shock & Vibration, 2006. **13**(4/5): p. 367-377.
3. Apud, H.E. and A.J. Brammer, *Effects of shock and vibration on humans.* Shock and Vibration handbook, 1998.
4. Committee, O.D.S., *Effect of vibration on buildings and their occupants-analysis of the literature and commentary*. 1982, Report no 4, Question D151: vibrations transmitted through the ground.
5. Hunt, H.E.M., *Measurement and modelling of traffic-induced ground vibration.* 1988.
6. Gordon, C.G. *Generic vibration criteria for vibration-sensitive equipment*. International Society for Optics and Photonics.
7. Hildebrand, R., *Countermeasures against railway ground and track vibrations.* 2001.
8. ; Available from: http://www.railsystem.net/track-structure/.
9. Wilson, G.P., H.J. Saurenman, and J.T. Nelson, *Control of ground-borne noise and vibration.* Journal of sound and vibration, 1983. **87**(2): p. 339-350.
10. Nelson, J.T., *Recent developments in ground-borne noise and vibration control.* Journal of sound and vibration, 1996. **193**(1): p. 367-376.
11. Saurenman, H. and J. Phillips, *In-service tests of the effectiveness of vibration control measures on the BART rail transit system.* Journal of Sound and Vibration, 2006. **293**(3-5): p. 888-900.

12. Vogiatzis, K.E. and G. Kouroussis, *Prediction and efficient control of vibration mitigation using floating slabs: practical application at Athens metro lines 2 and 3.* International Journal of Rail Transportation, 2015. **3**(4): p. 215-232.

13. Forrest, J.A. and H.E.M. Hunt, *Ground vibration generated by trains in underground tunnels.* Journal of Sound and Vibration, 2006. **294**(4-5): p. 706-736.

14. Hetenyi, M., *Beams on elastic foundation, 1946.* Ann Arbor: University of Michigan Press.

15. Kerr, A.D., *On the vertical modulus in the standard railway track analysis.* Rail International, 1987(11).

16. Han, S.M., H. Benaroya, and T. Wei, *Dynamics of transversely vibrating beams using four engineering theories.* Journal of Sound and vibration, 1999. **225**(5): p. 935-988.

17. Knothe, K. and S. Grassie, *Modelling of railway track and vehicle/track interaction at high frequencies.* Vehicle system dynamics, 1993. **22**(3-4): p. 209-262.

18. Bauchau, O. and J. Craig, *Euler-Bernoulli beam theory*, in *Structural analysis*. 2009, Springer. p. 173-221.

19. Lord, R., *The theory of sound*. 1945, Dover, New York.

20. Timoshenko, S.P., *LXVI. On the correction for shear of the differential equation for transverse vibrations of prismatic bars.* The London, Edinburgh, and Dublin Philosophical Magazine and Journal of Science, 1921. **41**(245): p. 744-746.

21. Timoshenko, S.P., *X. On the transverse vibrations of bars of uniform cross-section.* The London, Edinburgh, and Dublin Philosophical Magazine and Journal of Science, 1922. **43**(253): p. 125-131.

22. Thompson, D., *Theoretical modelling of wheel-rail noise generation.* Proceedings of the Institution of Mechanical Engineers, Part F: Journal of Rail and Rapid Transit, 1991. **205**(2): p. 137-149.

23. Thompson, D., *Railway noise and vibration: mechanisms, modelling and means of control*. 2008: Elsevier.

24. Thompson, D., *Wheel-rail noise generation, part I: introduction and interaction model.* Journal of sound and vibration, 1993. **161**(3): p. 387-400.

25. Chonan, S., *Moving harmonic load on an elastically supported Timoshenko beam.* ZAMM-Journal of Applied Mathematics and Mechanics/Zeitschrift für Angewandte Mathematik und Mechanik, 1978. **58**(1): p. 9-15.

26. Bogacz, R., T. Krzyýński, and K. Popp, *On the generalization of Mathews' problem of the vibrations of a beam on elastic foundation.* ZAMM-Journal of Applied Mathematics and Mechanics/Zeitschrift für Angewandte Mathematik und Mechanik, 1989. **69**(8): p. 243-252.

27. Mathews, P.M., *Vibrations of a beam on elastic foundation.* ZAMM-Journal of Applied Mathematics and Mechanics/Zeitschrift für Angewandte Mathematik und Mechanik, 1958. **38**(3-4): p. 105-115.

28. Mathews, P.M., *Vibrations of a beam on elastic foundation II.* ZAMM-Journal of Applied Mathematics and Mechanics/Zeitschrift für Angewandte Mathematik und Mechanik, 1959. **39**(1-2): p. 13-19.

29. Kenney, J.T., *Steady-state vibrations of beam on elastic foundation for moving load.* Journal of applied mechanics-Transactions of the ASME, 1954. **21**(4): p. 359-364.

30. Dörr, J., *Der unendliche, federnd gebettete Balken unter dem Einflu\einer gleichförmig bewegten Last.* Ingenieur-Archiv, 1943. **14**(3): p. 167-192.

31. Ludwig, K. *Deformation of rail elastically supported of infinite length by loads moving at a constant horizontal velocity*.

32. Hovey, B.K., *Beitrag zur Dynamik des geraden Eisenbahngeleises*. 1933: Göttingen.

33. Duffy, D.G., *The response of an infinite railroad track to a moving, vibrating mass*. Journal of Applied Mechanics, 1990. **57**(1): p. 66-73.

34. Fryba, L., *Vibration of solids and structures under moving loads,(1972).* Academia, Prague.

35. Kim, S.-M. and J.M. Roesset, *Dynamic response of a beam on a frequency-independent damped elastic foundation to moving load.* Canadian Journal of Civil Engineering, 2003. **30**(2): p. 460-467.

36. Mead, D., *Wave propagation and natural modes in periodic systems: I. Mono-coupled systems.* Journal of Sound and Vibration, 1975. **40**(1): p. 1-18.

37. Mead, D., *Wave propagation and natural modes in periodic systems: II. Multi-coupled systems, with and without damping.* Journal of Sound and Vibration, 1975. **40**(1): p. 19-39.

38. Jezequel, L., *Response of periodic systems to a moving load.* Journal of Applied Mechanics, 1981. **48**(3): p. 613-618.

39. Kisilowski, J., B. Sowiński, and Z. Strzyżakowski, *Application of Discrete-Continuous Model Systems in Investigating Dynamics of Wheelset-Track System Vertical Vibrations.* ZAMM-Zeitschrift fur Angewandte Mathematik und Mechanik, 1988(68).

40. Ilias, H. and S. Müller, *A discrete-continuous track-model for wheelsets rolling over short wavelength sinusoidal rail irregularities.* Vehicle System Dynamics, 1994. **23**(S1): p. 221-233.

41. KrzyŻYŃSki, T., *On continuous subsystem modelling in the dynamic interaction problem of a train-track-system.* Vehicle System Dynamics, 1995. **24**(sup1): p. 311-324.

42. MÜLler, S., T. KrzyŻYŃSki, and H. Ilias, *Comparison of semi-analytical methods of analysing periodic structures under a moving load.* Vehicle System Dynamics, 1995. **24**(sup1): p. 325-339.

43. Hildebrand, R., *Vertical vibration attenuation in railway track: a wave approach.* Journal of sound and vibration, 2001. **247**(5): p. 857-874.

44. Nordborg, A., *Vertical rail vibrations: Pointforce excitation.* Acta Acustica united with Acustica, 1998. **84**(2): p. 280-288.

45. Nordborg, A., *Vertical rail vibrations: parametric excitation.* Acta Acustica united with Acustica, 1998. **84**(2): p. 289-300.

46. Smith, C.C. and D.N. Wormley, *Response of continuous periodically supported guideway beams to traveling vehicle loads.* Journal of Dynamic Systems, Measurement, and Control, 1975. **97**(1): p. 21-29.

47. Smith, C., A. Gilchrist, and D. Wormley, *Multiple and continuous span elevated guideway-vehicle dynamic performance.* Journal of Dynamic Systems, Measurement, and Control, 1975. **97**(1): p. 30-40.

48. Belotserkovskiy, P.M., *Forced oscillations of infinite periodic structures. Applications to railway track dynamics.* Vehicle System Dynamics, 1998. **29**(S1): p. 85-103.

49. Kessel, P., *Resonances excited in an elastically connected double-beam system by a cyclic moving load.* The Journal of the Acoustical Society of America, 1966. **40**(3): p. 684-687.

50. Vu, H., A. Ordonez, and B. Karnopp, *Vibration of a double-beam system.* Journal of Sound and Vibration, 2000. **229**(4): p. 807-822.

51. Chen, Y.-H. and Z.-M. Shiu, *Resonant curves of an elevated railway to harmonic moving loads.* International Journal of Structural Stability and Dynamics, 2004. **4**(02): p. 237-257.

52. Forrest, J.A., *Modelling of ground vibration from underground railways*. 1999, University of Cambridge.

53. Samavedam, G. and P. Cross, *Dynamic analyses of vibration isolating tracks for tunnels*. 1980, Railway Technical Centre: Derby, England.

54. Cui, F. and C. Chew, *The effectiveness of floating slab track system—Part I. Receptance methods.* Applied Acoustics, 2000. **61**(4): p. 441-453.

55. Hussein, M.F.M. and H.E.M. Hunt, *Modelling of floating-slab tracks with continuous slabs under oscillating moving loads.* Journal of Sound and Vibration, 2006. **297**(1-2): p. 37-54.

56. Hussein, M.F.M. and H.E.M. Hunt, *Modelling of Floating-Slab Track with Discontinuous Slab: Part 1: Response to Oscillating Moving Loads.* Journal of low frequency noise, vibration and active control, 2006. **25**(1): p. 23-39.

57. Hussein, M.F.M. and H.E.M. Hunt, *Modelling of floating-slab track with discontinuous slab Part 2: Response to moving trains.* Journal of Low Frequency Noise Vibration and Active Control, 2006. **25**(2): p. 111-118.

58. Hussein, M.F.M. and P. A. Costa, *The effect of end bearings on the dynamic behaviour of floating-slab tracks with discrete slab units.* International Journal of Rail Transportation, 2017. **5**(1): p. 38-46.

59. Yang, J., et al., *Dynamic analysis on stiffness enhancement measures of slab end for discontinuous floating-slab track.* Computing in Science & Engineering, 2018.

60. Wei, G., et al., *Effect of dowel joints on dynamic behavior of train–discrete floating slab track system.* Advances in Mechanical Engineering, 2018. **10**(3): p. 1687814018767010.

61. Rücker, W., *Measurement and evaluation of random vibrations.* 1977.

62. Line, J., *London Transport Office of the Scientific Advisor.* Vibration Measurement at baker Street, 1982.

63. Zhenguang, P.C.X., *MEASUREMENT AND ANALYSIS OF VIBRATIONS CAUSED BY PASSING TRAINS IN SUBWAY RUNNING TUNNEL [J]*. China Civil Engineering Journal, 1990. **2**: p. 002.

64. Wolf, S., *Potential low frequency ground vibration (< 6.3 Hz) impacts from underground LRT operations.* Journal of sound and vibration, 2003. **267**(3): p. 651-661.

65. Liu, W.N., Zhang, H.R., Li, R.D., *Environmental Vibration Measurements in Beijing Metro Line*

1. 2005, Beijing Jiaotong University: Beijing,

China.

66. Degrande, G., et al., *Vibrations due to a test train at variable speeds in a deep bored tunnel embedded in London clay.* Journal of Sound and Vibration, 2006. **293**(3-5): p. 626-644.

67. Ding, D.-y., et al., *Low frequency vibration tests on a floating slab track in an underground laboratory.* Journal of Zhejiang University-SCIENCE A, 2011. **12**(5): p. 345-359.

68. Montella, G., A. Calabrese, and G. Serino. *Experimental and numerical investigations on innovative floating-slab track including recycled rubber elements*.

69. Jin, H., W. Liu, and S. Zhou, *1750. An experiment to assess vibration reduction ability of the rubber floating-slab tracks with different supporting forms.* Journal of Vibroengineering, 2015. **17**(6).

70. Zhu, S., et al., *Development of a vibration attenuation track at low frequencies for urban rail transit.* Computer-Aided Civil and Infrastructure Engineering, 2017. **32**(9): p. 713-726.

71. Zhao, C. and W. Ping, *Minimizing noise from metro viaduct railway lines by means of elastic mats and fully closed noise barriers.* Proceedings of the Institution of Mechanical Engineers, Part F: Journal of Rail and Rapid Transit, 2018: p. 0954409717752200.

72. 6.14-1., A.C.v. and R.I. Providence, Dassault Systèmes, 2014 .

73. *L. Meirovitch, Elements of Vibration Analysis, 2nd ed., McGraw-Hill, New York, 1986.*

74. 8.1.0.604., M.v. and M.T.M.I. Natick, 2013.

75. Vibrant Technology, I. and S.V. (2015). "ME'ScopeVES 6.0", California.

76. Ewins, D.J., *Modal testing: theory and practice*. Vol. 15. 1984: Research studies press Letchworth.

77. Konak, A., D.W. Coit, and A.E. Smith, *Multi-objective optimization using genetic algorithms: A tutorial.* Reliability Engineering & System Safety, 2006. **91**(9): p. 992-1007.

78. Blevins, R.D. and R. Plunkett, *Formulas for natural frequency and mode shape.* Journal of Applied Mechanics, 1980. **47**: p. 461.